Effect of pulsed metal inert gas (pulsed-MIG) and cold metal transfer (CMT) techniques on hydrogen dissolution in wire arc additive manufacturing (WAAM) of aluminium

Derekar, K., Addison, A., Joshi, S., Zhang, X., Lawrence, J., Xu, L., Melton, G. & Griffiths, D.

Effect of pulsed metal inert gas (pulsed-MIG) and cold metal transfer (CMT) techniques on hydrogen dissolution in wire arc additive manufacturing (WAAM) of aluminium

Karan S. Derekar[1,2,a]*, Adrian Addison[3,b], Sameehan S. Joshi[4,c], Xiang Zhang[1,d], Jonathan Lawrence[1,e], Lei Xu[3,f], Geoff Melton[3,g], David Griffiths[3,h]

Address:
[1]Faculty of Engineering, Environment and Computing, Coventry University, Coventry, CV1 5FB, UK,
[2]National Structural Integrity Research Centre (NSIRC), TWI Ltd, Granta Park, Great Abington, Cambridge, CB21 6AL, UK,
[3]TWI Ltd, Granta Park, Great Abington, Cambridge, CB21 6AL, UK
[4]Department of Materials Science and Engineering, University of North Texas, 1150 Union Circle 305310, Denton, TX 76203-5017, USA

[a]derekark@uni.coventry.ac.uk, [b]adrian.addison@twi.co.uk, [c]sameehanjoshi@gmail.com, [d]xiang.zhang@coventry.ac.uk, [e]ac5588@coventry.ac.uk, [f]lei.xu@twi.co.uk, [g]geoff.melton@twi.co.uk, [h]david.griffiths@twi.co.uk,

*Corresponding author
Karan S. Derekar[1,2,a]
[1]Faculty of Engineering, Environment and Computing, Coventry University, Coventry, CV1 5FB, UK,
[2]National Structural Integrity Research Centre (NSIRC), Granta Park, Great Abington, Cambridge, CB21 6AL, UK,
[a]derekark@uni.coventry.ac.uk
ORCID – 0000-0003-3909-5337

Abstract

Aluminium is one of the most experimented metals in the WAAM field owing to a wide range of applications in the automotive sector. Due to concerns over reduction of strength, elimination of porosity from wire arc additive manufactured aluminium is one of the major challenges. In line with this, the current investigation presents findings on hydrogen dissolution in solid aluminium and hydrogen consumed to form porosity along with its distribution as a function of heat inputs and interlayer temperatures in a WAAM 5183 aluminium alloy. Two varieties of WAAM, pulsed metal inert gas (MIG) and cold metal transfer (CMT) were explored. Samples made with pulsed metal inert gas (pulsed MIG) process picked up more hydrogen compared to samples produced by cold metal transfer technique. Correspondingly, pulsed MIG samples showed increased number of pores and volume fraction of porosity than samples manufactured using the cold metal transfer (CMT) technique for different heat input and interlayer temperature conditions. However, CMT samples exhibited higher amount of dissolved hydrogen in solid solution compared to pulsed MIG process. In addition, heat input, interlayer temperature and interlayer dwell time also played a key role in pore formation and distribution in WAAM produced aluminium 5183 alloy.

Keywords: Wire arc additive manufacturing (WAAM), aluminium, porosity, hydrogen dissolution, interlayer temperature, cold metal transfer (CMT), pulsed metal inert gas (pulsed-MIG)

Acknowledgements

1. Introduction –

Wire arc additive manufacturing (WAAM) as a developing technique has attracted the attention of many researchers and industry personnel alike owing to its high deposition rate, flexibility in operation and possibility of part production without dimensional limits [1–4]. High cost materials such as Ti-6Al-4V and Inconel possess better business case for using WAAM than conventional process owing to process advantages, significant material savings, and their applications in the aerospace sector. Microstructural features, mechanical properties and in-situ product finishing techniques are the areas of interests [5–7]. Different microstructural features and relatively reduced mechanical properties compared to conventionally processed wrought products and management of residual stresses are the challenges to industrialisation of the WAAM technique [1,3,8–10].

Lower cost alloys such as aluminium have also been studied owing to its widespread applications in the automotive and aerospace sectors. Apart from the aforementioned challenges, porosity formation due to hydrogen pick up [11,12] and inter granular cracking [13] are commonly found in WAAM aluminium parts. Porosity formation in aluminium refers to the large difference between the solubility limit of hydrogen in solid and liquid aluminium (0.4 ml/kg in solid and 7 ml/kg in liquid [14]). Major sources of hydrogen are moisture, grease and other hydrocarbons [11,15,16] that come from the surface of filler wire. Contamination and moisture from shielding gas, hose, tube and substrate can also add to the total hydrogen content. Lastly, dissolved hydrogen is present in the wire and substrate. Hydrogen from contaminants immediately converts into atomic hydrogen and is readily absorbed in-to the liquid aluminium [16]. Use of dip metal transfer techniques such as the cold metal transfer (CMT) has proven its applicability in reducing the overall porosity content due to peculiar metal deposition mode and relatively low heat input obtained by electronically and mechanically controlled metal deposition [1,11,12] compared to conventional pulsed metal inert gas (MIG) process. The technique was studied for welding of thin plates and minimal dilution cladding of aluminium plates because of increased control on metal droplet transfer mode and low dilution. Along with CMT, application of interlayer rolling has found beneficial effects in terms of reducing porosity content as well as achieving preferable microstructure [7,8,11].

Due to repeated application of heat in layered metal deposition, the deposit undergoes repeated reheating that affects microstructure, mechanical properties and residual stresses in a formed component [1,3,8,9]. Thus, in robotic metal deposition temperature control and heat management are crucial factors to achieve optimal material properties. In robotic operation, layer initiation is usually controlled by a fixed interlayer dwell time [8,11], however, depending on the size and shape of the forming part, interlayer waiting time does not account for or provide sufficient control over temperature. Thus, inter layer temperature i.e. the temperature of the top layer immediately before deposition of a successive layer, could be the reasonable variable to control the temperature. Geng et al [17] used the similar approach for achieving better layer appearance using between 50 to 80°C for the first layer and 120°C for subsequent layers. The results complied with the welding standard BS EN 1011-4:2000 that suggests maximum interpass temperature of 120°C for 5xxx series aluminium welding consumables.

In his paper, the effects of different deposition conditions, namely the heat input, interlayer temperature and interlayer dwell time, on porosity formation and distribution are

studied. The results of pulsed MIG and CMT processed samples are compared with respect to hydrogen dissolution and metal deposition techniques.

2. Experimental approach

2.1 Materials and consumables

Solid wire ER5183 was used for manufacturing of a WAAM part on a wrought plate substrate with dimension 200 x 125 x 20 mm3 made of Al-Mg-Mn alloy. Nominal chemical compositions of the materials are provided in Table 1. Commercially available argon gas with purity of 99.998% (trade name - Argon Technical, supplied by Air Products and Chemical Inc.), was used in this study. During metal deposition, the substrate was clamped firmly to the welding platform to avoid any possible distortion. Apart from the elements listed in Table 1, authors performed hydrogen analysis and found that the hydrogen content in feed stock wire was ~ 7.5 ppm/100gm of metal. The wire samples were thoroughly cleaned and dried before analysis. It is worth mentioning here that the detected hydrogen content in wire can be skewed because of surface organic contaminants. It has been reported that attributes such as surface irregularities/roughness features may help retaining the organic matter[18,19]

Table 1 Nominal chemical composition of depositing wire and substrate (in weight percentage)

Elements	Si	Mn	Cr	Cu	Ti	Fe	Zn	Mg	Al
Filler wire	0.06	0.65	0.07	0.01	0.07	0.14	<0.01	4.91	Balance
Substrate	0.11	0.66	0.06	0.05	0.05	0.25	0.05	4.74	Balance

2.2 Sample manufacturing

In order to study the effects of different deposition parameters on porosity distribution, eight samples were manufactured using conventional pulsed MIG and another eight were prepared using CMT. Fig 1 describes the operation and sequence of metal deposition used in this experimentation. An OTC Daihen Synchrofeed welding setup (Fig 2a) was used to deposit the part with pulsed MIG process and a Fronius TPS400i CMT Advanced power source integrated with Fanuc robot (Fig 2b) was employed for manufacturing of CMT samples. Two heat input values, minimum and maximum, were selected for both techniques based on previous study at TWI Ltd. (Table 2 gives deposition parameters). The mentioned values in Table 2 were obtained from averaging values over roughly 5 seconds (approx. 25000 instantaneous values) of stable metal deposition mode. Heat input calculations were based on equations (1) and (2) described by [1,20]. Parameters such as current, voltage and heat input variation are shown in graphical format in Fig 3 where high frequency represented maximum heat input compared to low frequency displaying minimum heat input. Each sample had a total of 15 layers and 100 mm in length.
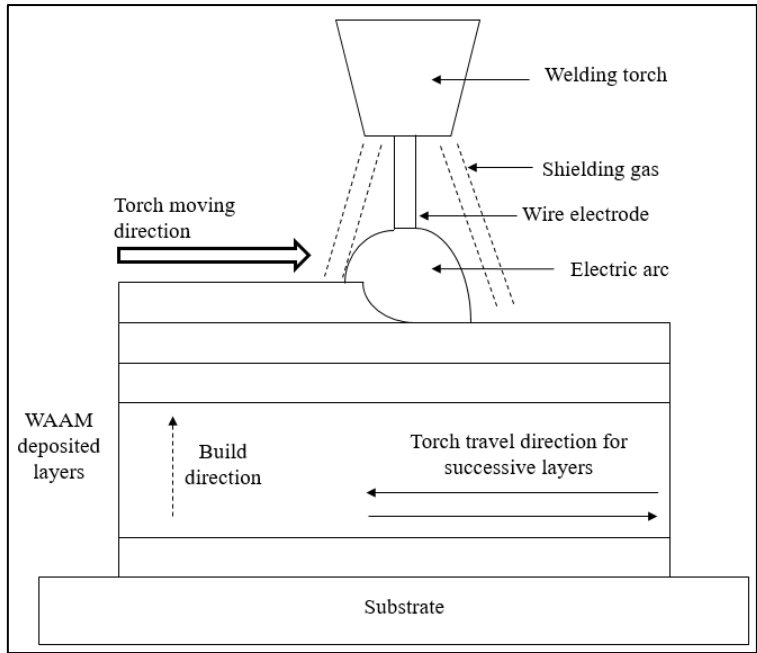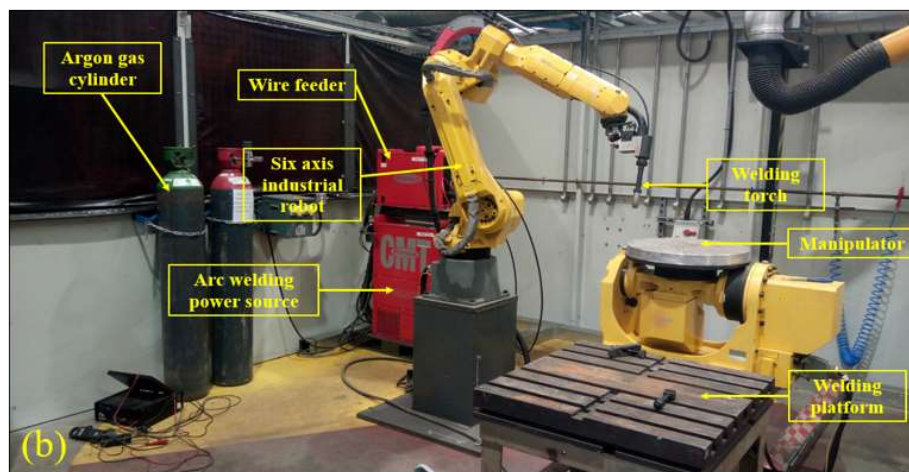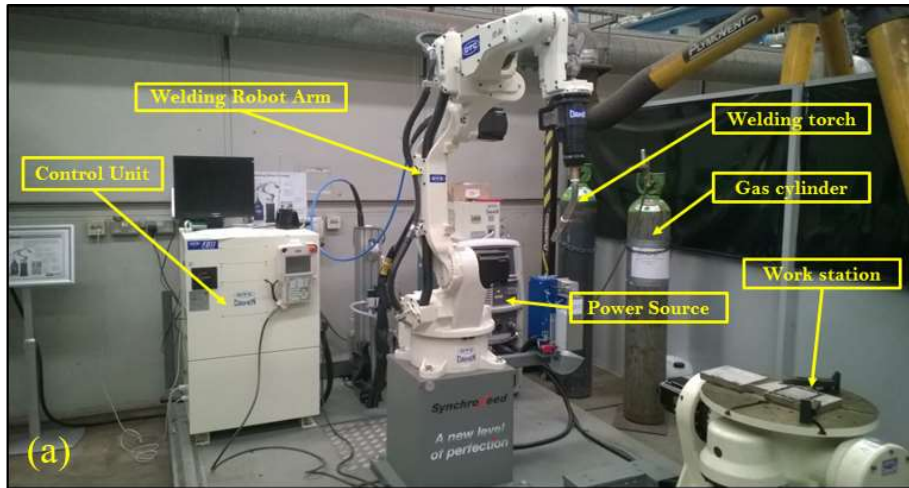
Fig 1 Schematic of WAAM deposition using gas metal arc technique

Fig 2 Welding robot (a) OTC Daihen Synchrofeed welding robot for pulsed metal inert gas (MIG) technique (b) Fronius CMT-Fanuc work station for cold metal transfer (CMT) technique

Table 2 Parameters employed for manufacturing of test samples

Parameter	Pulsed metal inert gas (MIG)		Cold metal transfer (CMT)	
	Low heat input	High heat input	Low heat input	High heat input
Average Current (A)	73	152	73	152
Average Voltage (V)	18.3	18.7	18.2	19.2
Torch travel speed (m/min)	0.6		0.6	
Heat input (J/mm)	158	351	140	345
Wire feed speed (m/min)	4.85	8.65	4.9	8.6
Wire feed speed / travel speed	8.1	14.4	8.1	14.3

$$Heat\ input = \eta\ \frac{Average\ voltage\ x\ Average\ current}{Travel\ speed} \qquad (1)$$

$$Heat\ input = \frac{\eta \sum_{i=1}^{n} \frac{Ii * Ui}{n}}{Travel\ speed} \qquad (2)$$

where η is efficiency of welding process, Ii and Ui are instantaneous current and voltage at an instant of time. From the literature, efficiency of the process (η) is 0.8 [21].
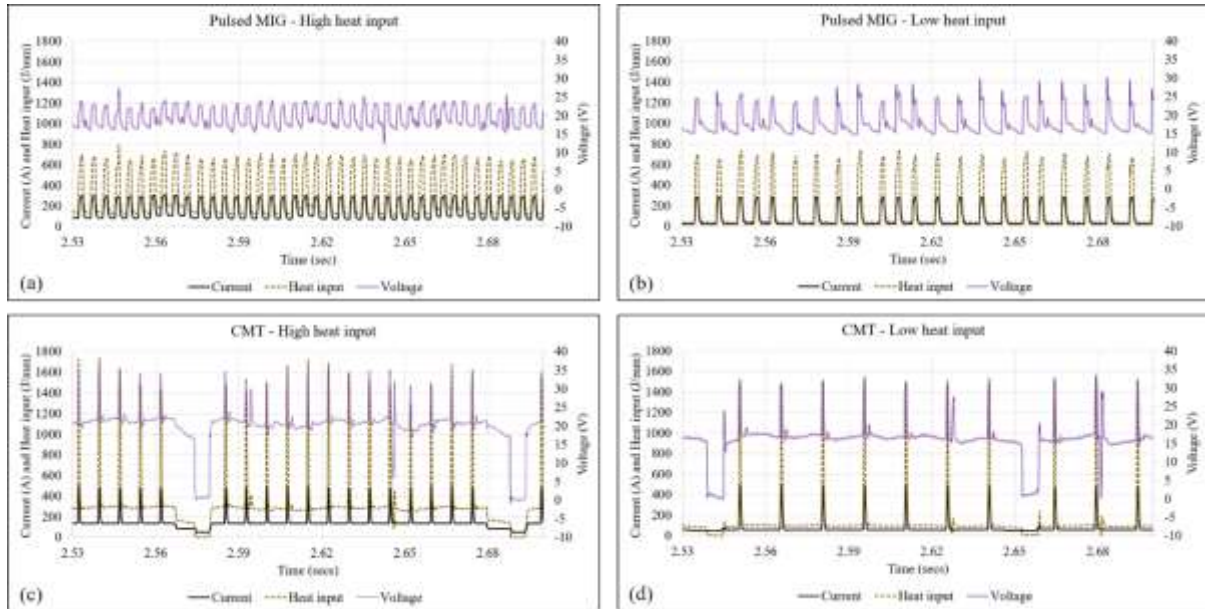
Fig 3 Current, voltage and heat input variations using (a) pulsed MIG high heat input (b) pulsed MIG low heat input (c) CMT high heat input and (d) CMT low heat input

Interlayer temperature controlled samples were manufactured with either 50°C or 100°C interlayer temperatures. Temperature measurement was performed using portable contact K-type digital thermometer. The choice of thermometer was based on guidelines given in ASTM E2877. During part manufacturing, only top layer was considered for temperature measurement. After layer deposition, temperature was measured using thermometer at three locations, the centre and approximately 25 mm from each end in 100 mm length. The deposition of successive layer was not initiated until the specified temperature, either 50°C or 100°C, was reached by natural cooling. Defined preheat was maintained at substrate for initial layers and was checked using the same thermometer. In this manner, a total of eight samples, four in set 1 and four in set 2, were prepared using pulsed MIG and CMT respectively as described in section 2.4 and Table 3. A robot program was developed with fixed interlayer dwell time without considering the interlayer temperature while depositing total 15 layers, for further eight samples with fixed interlayer dwell time of either 30 or 120 seconds using the two metal deposition techniques and two heat inputs, identified as sets 3 and 4, as described in section 2.4 and Table 3. To minimise the dissimilarities between the processed samples from CMT and pulsed MIG process, feed stock material was consistent (same spool) for all the samples and manufacturing experiments were conducted in a laboratory with controlled conditions i.e. temperature and humidity.

2.3 Testing

After manufacturing a total of 16 samples, a part of approximately 35 mm length representing stable deposition conditions was cut from the end of each sample. Each part

having approximately 7200 mm^3 volume was scanned with X-ray Computed Tomography (XCT) using a HMX 225 system. Operation and data acquisition were controlled by X-Tek InspectX software and VGStudioMAx software was used for visualisation.

Following the XCT, a part of the samples was cut from the stable deposition condition for hydrogen dissolution test. Two samples from pulsed MIG were selected along with similarly processed two CMT samples as discussed in Table 6 and 7. Total hydrogen in a sample was tested using Leco RH402 instrument. Small part of the samples from XCT scanned area was used for hydrogen detection test. The samples were tested for all the available hydrogen in samples, dissolved and entrapped state. For pore comparison and analysis, approximately 2000 mm^3 part of stable metal deposition was considered.

2.4 Sample identification

The study included total 16 different types of samples. For simplicity and convenience, samples were given identification names (ID). First letter in the ID refers to the deposition process. CMT is denoted by letter 'C' and pulsed MIG by letter 'P'. The middle letters refer to the heat input. 'HH' for high heat and 'LH' for low heat. The last letter refers to either the interlayer temperature or interlayer dwell time. 'T1' and 'T2' represent the 50°C and 100°C interlayer temperature respectively whilst 't1' and 't2' denote the interlayer dwell time of 30 and 120 seconds respectively. For example, C-HH-T1 represents the sample built by CMT technique with high heat input and 50°C interlayer temperature, P-LH-t1 denotes the sample built by pulsed MIG with low heat input and 30 seconds of interlayer dwell time. Samples manufactured using similar deposition conditions were grouped into four categories as described in Table 3. Sets 1 and 2 represent samples manufactured with interlayer temperature control (interlayer dwell time not considered), while Sets 3 and 4 include samples prepared using specific interlayer dwell times (interlayer temperature not considered).

Table 3 Sample identification and set groups

Set no.	Metal deposition technique	Heat input	Interlayer temperature (T) / Interlayer dwell time (t)	Samples
1	Pulsed MIG (P)	High (HH) Low (LH)	50°C (T1) 100°C (T2)	P-HH-T1, P-HH-T2, P-LH-T1, P-LH-T2
2	CMT (C)	High (HH) Low (LH)	50°C (T1) 100°C (T2)	C-HH-T1, C-HH-T2, C-LH-T1, C-LH-T2
3	Pulsed MIG (P)	High (HH) Low (LH)	30 secs (t1) 120 secs (t2)	P-HH-t1, P-HH-t2, P-LH-t1, P-LH-t2
4	CMT (C)	High (HH) Low (LH)	30 secs (t1) 120 secs (t2)	C-HH-t1, C-HH-t2, C-LH-t1, C-LH-t2

3. Results

3.1 Volume consideration

XCT scan images of two samples, C-HH-T2 and P-HH-T2, are shown in Fig 4 a and b respectively. Similar images and porosity distribution data were obtained from all 16 samples as mentioned in section 2.2. From Fig 4 a and b it was apparent that porosity population was increased in the areas of arc start and arc stop. Since these two areas are usually removed from

final component by machining, they were omitted from the analysis. An area representing stable deposition condition which was more than 15 mm away from the ends and 6 mm above the substrate was chosen for detailed analysis. Representative micrographs taken on YZ plane of C-HH-T2 and P-HH-T2 samples are shown in Fig 4 c and d.
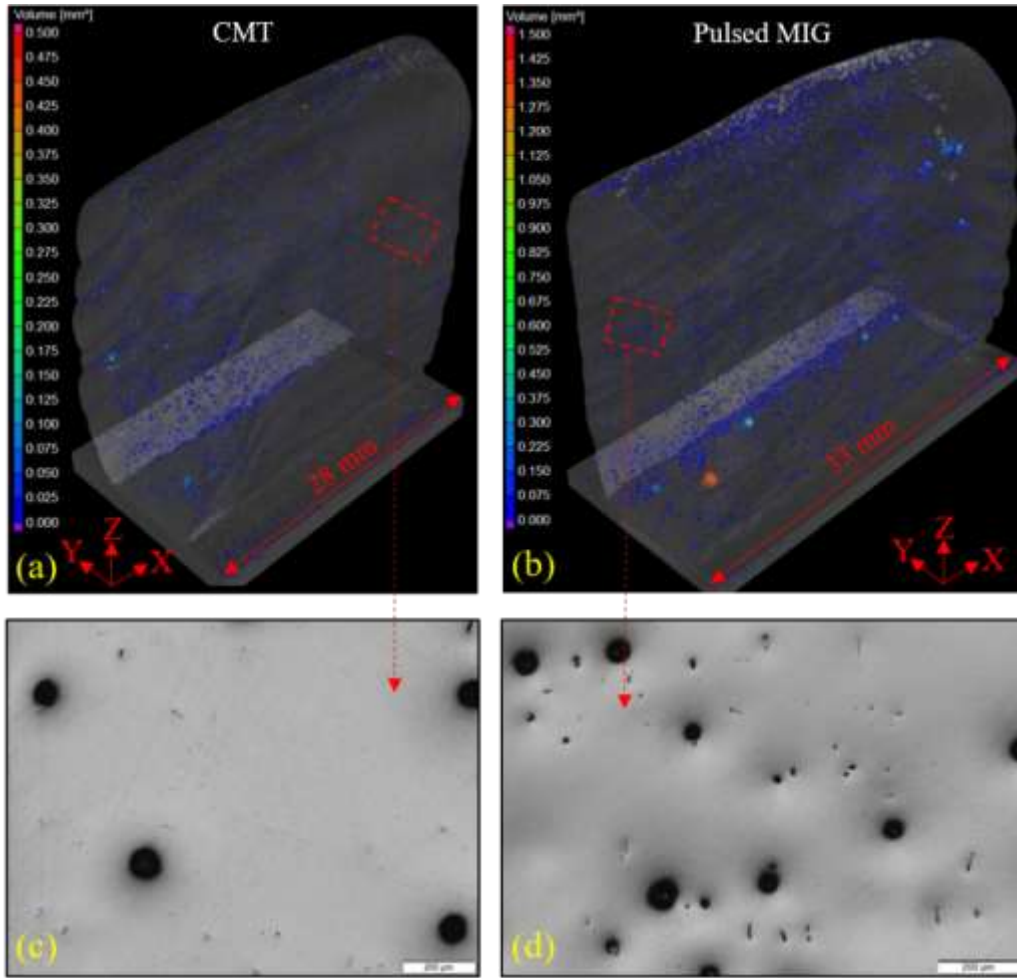
Fig 4 X-ray computed tomography of Samples (a) C-HH-T2 and (b) P-HH-T2. Micrographs showing porosity morphology in respective samples (c) C-HH-T2 and (d) P-HH-T2

3.2 Comparison of overall porosity content

3.2.1 Effect of process techniques (Pulsed MIG vs. CMT)

Mode of metal deposition showed major effect on the pore content. Samples prepared using CMT generally showed lower pore volume compared with samples manufactured using pulsed MIG. Table 4 gives the respective deposition conditions such as interlayer temperature, interlayer dwell time and heat input. As expected, the low heat input, high frequency oscillating wire and dip transfer effects of CMT resulted in less porosity [12,22] than pulsed MIG. The smallest difference of 10% in the porosity content between CMT and pulsed MIG was observed in the samples manufactured with high heat input and 100°C interlayer temperature (C-HH-T2 and P-HH-T2). On the other hand, the largest difference of 390% was noted for the samples manufactured with low heat input and 50°C interlayer temperature (C-LH-T1 and P-LH-T1).

Samples with low heat input and 120 secs of interlayer dwell time (C-LH-t2 and P-LH-t2) also showed a significant difference of 360% in the pore content between CMT and pulsed MIG techniques. Only the pulsed MIG sample with high heat input and 30 seconds interlayer dwell time (P-HH-t1) showed less porosity than an equivalent CMT based sample (C-HH-t1) by 6%.

Table 4 Pore volume fraction for samples manufactured with different interlayer temperatures (sets 1 and 2) or with different interlayer dwell time (Sets 3 and 4)

Process	Heat input	Sample ID	Pore volume fraction % with respect to sample volume
Pulsed MIG (Set 1)	High	P-HH-T1	0.106
		P-HH-T2	0.063
	Low	P-LH-T1	0.152
		P-LH-T2	0.122
CMT (Set 2)	High	C-HH-T1	0.05
		C-HH-T2	0.057
	Low	C-LH-T1	0.031
		C-LH-T2	0.041
Pulsed MIG (Set 3)	High	P-HH-t1	0.066
		P-HH-t2	0.127
	Low	P-LH-t1	0.077
		P-LH-t2	0.175
CMT (Set 4)	High	C-HH-t1	0.07
		C-HH-t2	0.061
	Low	C-LH-t1	0.049
		C-LH-t2	0.038

3.2.2 Effect of heat input

The effect of heat input on porosity content was opposite between CMT and pulsed MIG when compared with similar process conditions. All samples manufactured with CMT showed increased porosity by total volume under high heat input compared to low heat input; this effect was maintained for two different interlayer temperature or two dwell time control conditions (refer Table 4). However, pulsed MIG samples manufactured with low heat input revealed more porosity by total volume fraction compared to high heat input samples as shown in Table 4. For the CMT samples, the difference in porosity volume fraction was the largest between the two 50°C interlayer temperature samples C-HH-T1 and C-LH-T1 (0.05% and 0.031% for high and low heat input respectively, resulting in 61.2% difference), and smallest for the C-HH-T2 and C-LH-T2 samples (0.057% and 0.041 % for high and low heat input respectively thus a difference of 39%). For pulsed MIG samples, largest difference of 93.6% was found between samples with 100°C interlayer temperature, P-LH-T2 and P-HH-T2 (0.122% and 0.063% for low and high heat input respectively) and smallest difference was 16.6% in the 30 secs interlayer dwell time samples, P-LH-t1 and P-HH-t1, (0.077% and 0.066% for low and high heat input respectively).

3.2.3 Effect of an interlayer temperature and dwell time

Interlayer temperature was also found to impact the overall porosity content. For the pulsed MIG samples, low interlayer temperature showed increased porosity content compared to high interlayer temperature samples for both the heat inputs. The porosity content difference was 68.2% and 24.5 % between the high and low heat input samples respectively (Table 4). However, for CMT samples, a reversed trend was found. High interlayer temperature processed samples such as C-HH-T2 and C-LH-T2 showed more porosity content than low interlayer temperature samples C-HH-T1 and C-LH-T1.

A similar trend was observed with samples with interlayer dwell time control. Pulsed MIG samples manufactured with 120 second interlayer dwell time showed higher pore content than 30 second interlayer dwell time, irrespective of the heat input. The difference was 92.4% and 127% for high and low heat input samples, respectively. For CMT samples, pore content was higher for 30 second interlayer dwell time than 120 seconds with a difference of 14.7% and 28.9% for high and low heat input respectively.
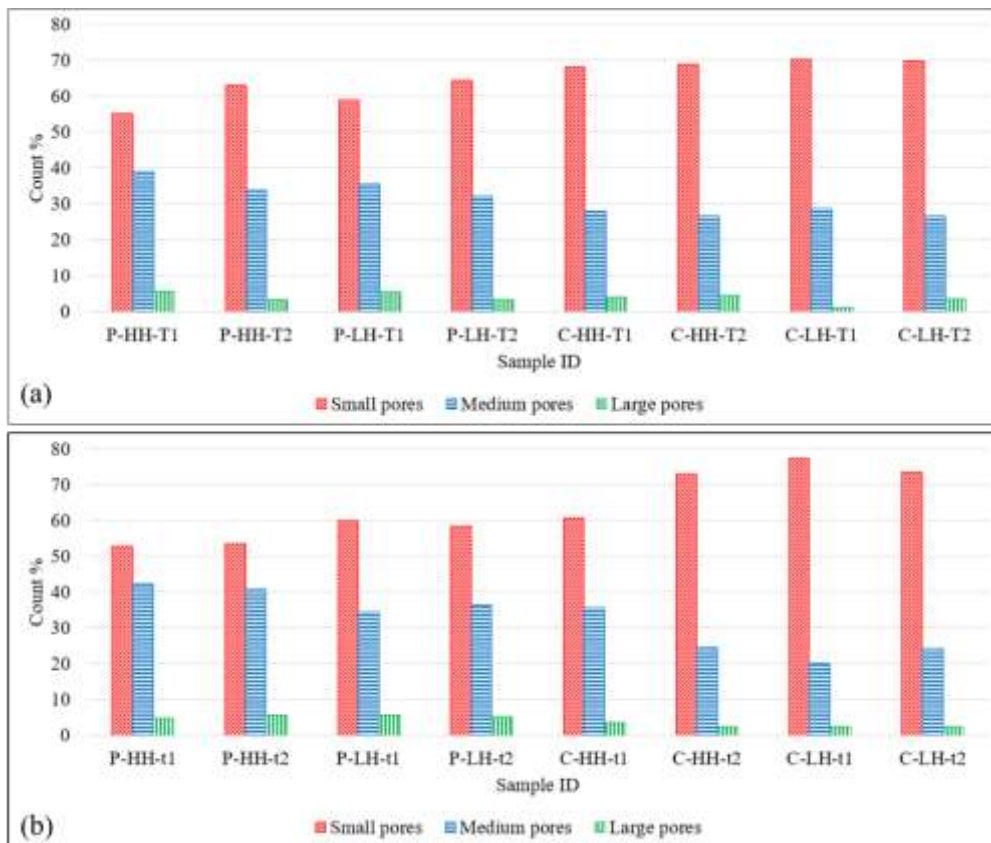
3.3 Pore size

Pore size within each sample was measured using the XCT scans and processing software to identify the distribution of size and relative percentages of the population. Pore smaller than 0.1 mm dimeter were not considered because they were found having negligible effect on fatigue life [23]. The remaining pores were split into three size ranges: small (0.11 – 0.20 mm), medium (0.21 – 0.30 mm) and large (larger than 0.31 mm). Table 5 shows the pore counts of each size range as a percentage of the total pore number detected for all 8 samples.

Table 5 Comparison of pore size range and distribution for pulsed MIG and CMT aluminium samples

Pore diameter range (mm)	Pore count fraction (%)	
	Pulsed MIG	CMT
Small (0.11 – 0.20)	52.79 – 62.9	60.69 – 77.47
Medium (0.21 – 0.30)	32.34 – 42.36	20.0 – 35.59
Large (≥ 0.31)	3.3 – 5.78	1.15 – 4.63

As shown in Table 5, CMT had comparatively higher population of small pores than pulsed MIG samples, whilst the opposite was found for the numbers of medium and large pores. Albeit with some small differences, this pattern was repeated with both interlayer temperature and interlayer dwell time controls as in Fig 5a and b. Irrespective of the deposition conditions, small pores dominated the size distribution with more than 50% of the total pore population as can be seen in Fig 5a and b. However, a significant number medium and large sized pores were also present. Samples manufactured by CMT showed a comparatively higher number of small sized pores ranging between 60.69 % and 77.47 % of the total number of pores, whereas; the same sized pore was varying between 52.79 % and 62.9 % for pulsed MIG samples. For CMT samples, medium sized pores were relatively fewer in count compared to pulsed MIG samples. Same sized pores in CMT processed samples were ranging between 20% and 35.5% while pulsed MIG samples showed between 32.2% and 42.3%. On the similar note, more pores with diameter greater than 0.31 mm were found in pulsed MIG processed samples (3.3% to 5.78 %) compared to CMT samples (1.15% to 4.63 %). Thus increased number of small pores in CMT samples reduced the number of larger pores compared to pulsed MIG samples.

1

Fig 5 Count of different porosity size ranges in the samples manufactured with (a) interlayer
temperature control and (b) interlayer dwell time control
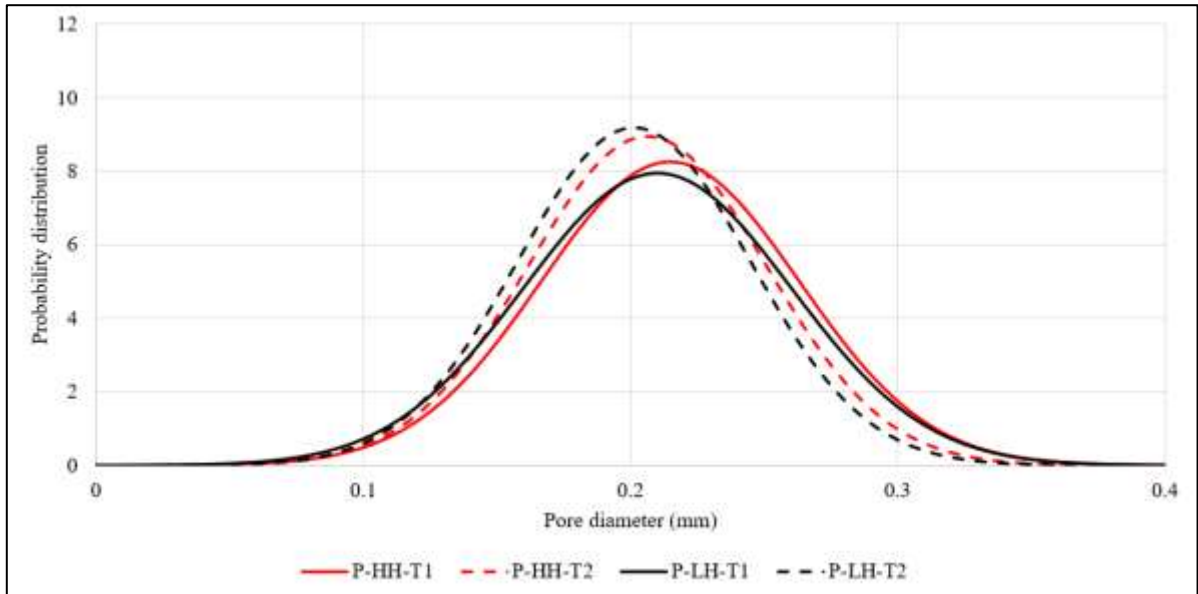
3.4 Pore size distribution

Pore size distribution was measured using the XCT scans results, which is shown in Fig
6 to Fig 9. Fig 6 illustrates the pore diameter distribution of CMT samples with low and high
heat input with consideration of interlayer temperatures. The average size of all pores, i.e. peak
of the curves, is approximately the same (0.2 mm), despite a slight increase in the average for
the high heat input samples. However, the pore size distribution of high heat input samples is
wider than those low heat input samples. Irrespective of the heat input, samples with high
interpass temperature showed wider variation in the pore diameter as compared to those made
with lower interpass temperature. This means that the samples made with high heat input and
high interlayer temperature had more irregularities in the pore sizes. When compared with

Fig **7** that shows pulsed MIG samples with similar conditions, the trends following
effect of the interlayer temperature was reversed. In the case of pulsed MIG, samples made
with lower interlayer temperature showed higher average pore size and variance implying that
low heat input and low interlayer temperature caused the most irregularities. However, the
difference in the average pore size (approx. 0.2 mm) between pulsed MIG and CMT was very
small.
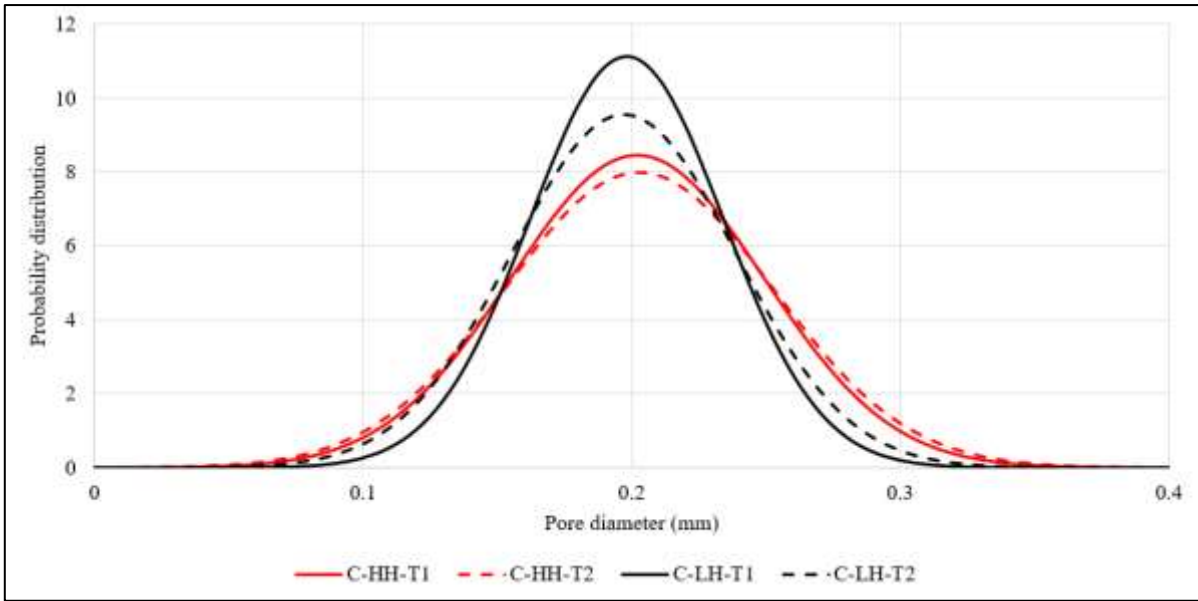
Fig 6 Effect of heat input and interlayer temperature on normal distribution of pore size in CMT samples (Set 2)

Fig 7 Effect of heat input and interlayer temperature on normal distribution of pore sizes in pulsed MIG samples (Set 1)

Pulsed MIG samples with high and low heat inputs did not reveal observable influence of interlayer dwell time as demonstrated by the overlapping curves in Fig 8 and Fig 9. Comparing the deposition techniques for both high and low heat input, pulsed MIG samples showed increased variance with pore size than CMT processed samples. Hence, samples prepared with CMT showed relatively smaller pore size and narrower pore size distribution. The average pore size was smaller in the CMT the pulsed MIG samples.
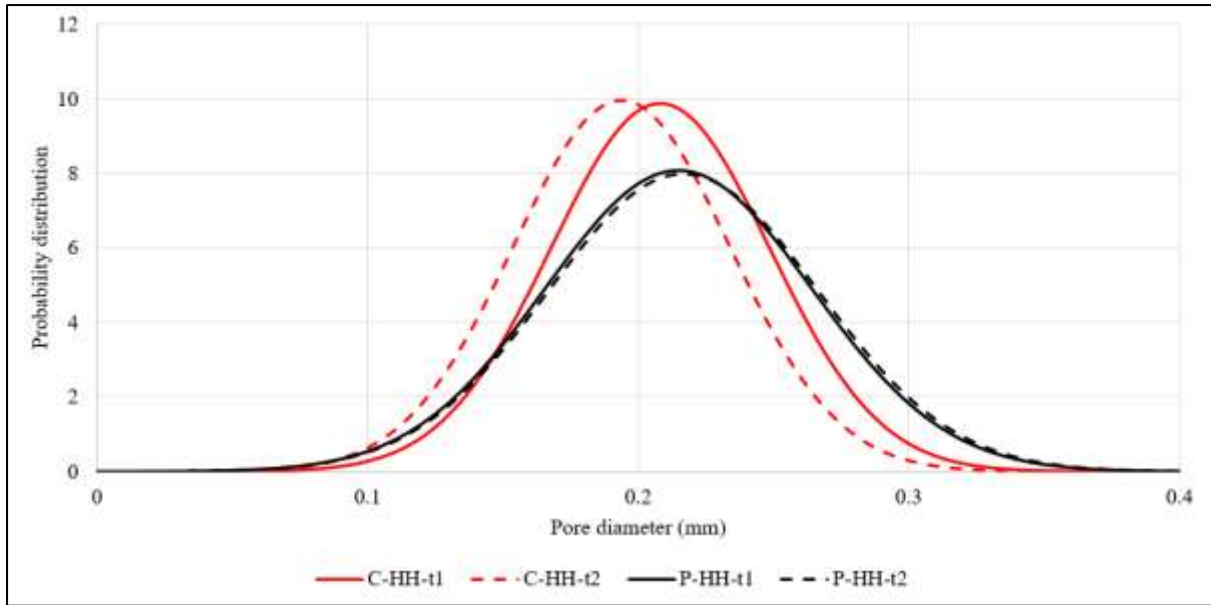
Fig 8 Effect metal deposition technique on normal distribution of pore size in samples manufactured with high heat input and different interlayer dwell times
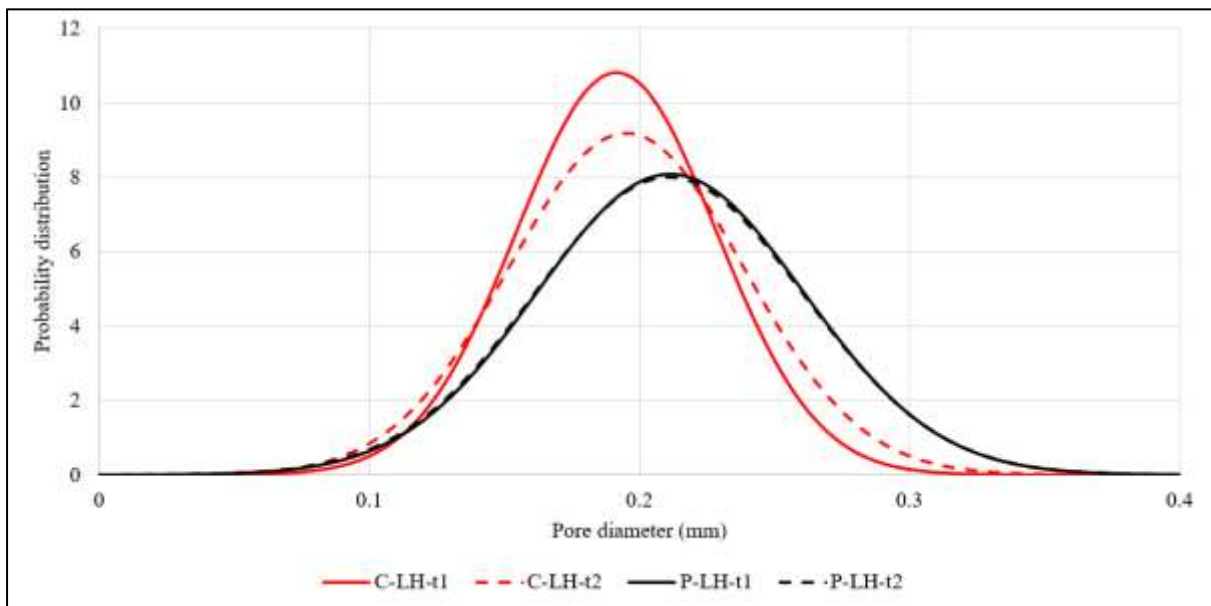
Fig 9 Effect metal deposition techniques on normal distribution of pore size in samples manufactured with low heat input and different interlayer dwell times

3.5 Average pore location and physical distribution

Comparison of a normalised distance of pores from the centroid of all pores is represented as a function of deposition process, interlayer temperature, interlayer dwell time and pore diameter in a normal distribution format in Fig 10 to Fig 13. Referring to Fig 10, for similar conditions, the average normalised distance from the centroid of all the pores was smaller for CMT than pulsed MIG, indicating that the pores were more concentrated within a small region in CMT. Additionally, the distribution of small pores on the normal distribution curve was comparatively wider for CMT, suggesting that the variance in the normalised distance of the pores was larger i.e. non uniform distribution of pores in the CMT samples. The

distribution of medium size pores was evidently wider than the smaller pores. Hence, there was a lower predictability in terms of number of pores within a small area considered for analysis. Irrespective of the size of the pores, their average normalised distance from the centroid was greater in pulsed MIG sample.
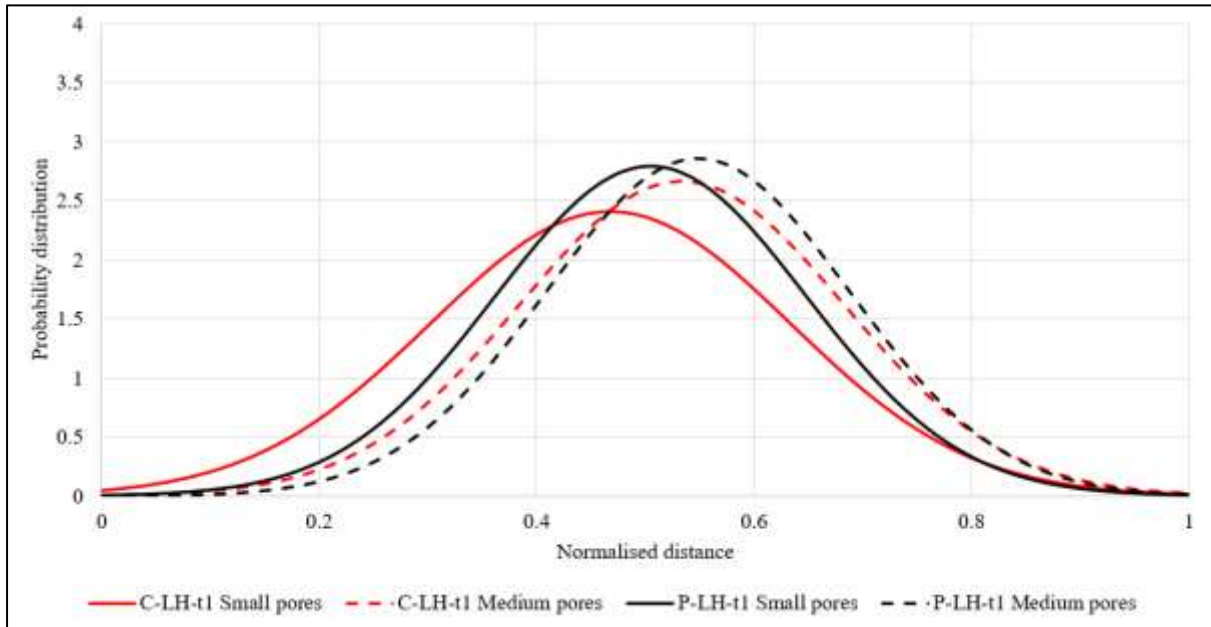
Fig 10 Effect of metal deposition technique on normal distribution of pore normalised distance between centroids

Fig 11 shows that for CMT samples, interlayer temperature affects pore size and its distribution. Irrespective of the pore size, samples processed with 50°C interlayer temperature showed smaller average normalised distance between the centroid of the pores compared to samples manufactured with 100°C interlayer temperature; hence, pores were more closely distributed in the lower interlayer temperature samples. Also, the lower interlayer temperature samples has less variance indicating that pores were more uniformly distributed compared to high interlayer temperature samples. Similar to Fig 10, medium size pores showed relatively greater average normalised distance between centroids and also an increased variance than small pores indicating large pores being less uniformly distributed along with wider distance.
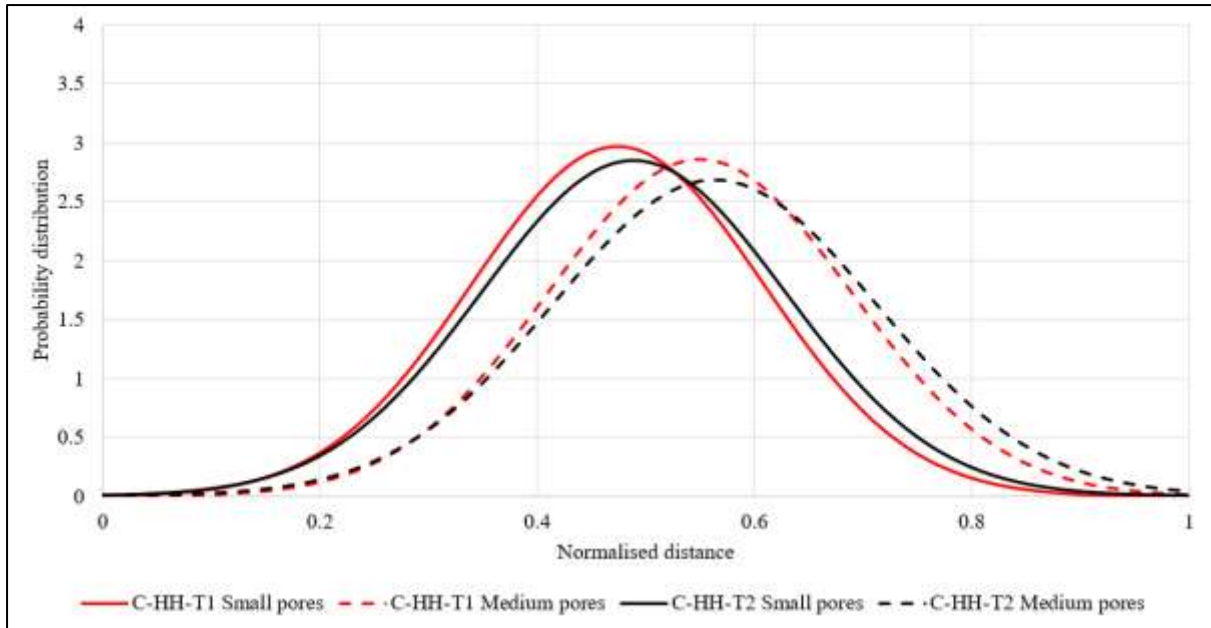
Fig 11 Effect of interlayer temperature on normal distribution of pore normalised distances from centroid of all pores

Following Fig 12 which compares the effect of heat input, medium size pores had relatively wide distribution than the small size pores irrespective of the heat inputs. The high heat input samples showed larger difference in the average normalised distance when grouped into small and large sized pores as compared to low heat input samples. For small pores, the difference in normalised distances was negligible, however, smaller pores exhibited more variance than the larger pores.
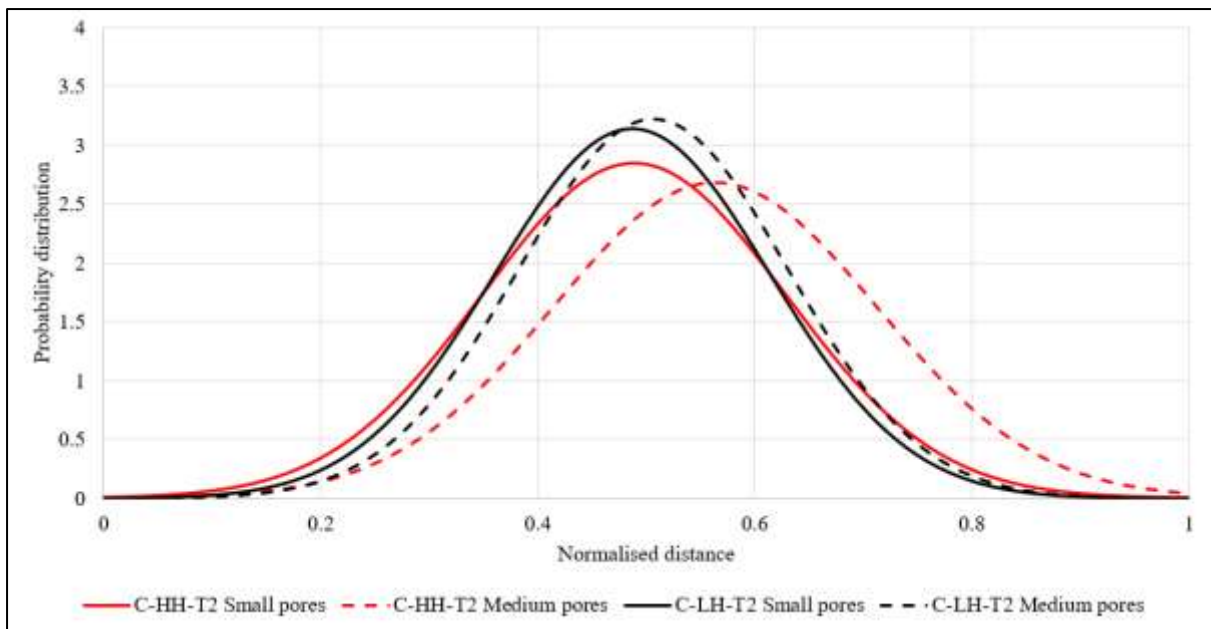

Fig 12 Effect of heat input on normal distribution of pore normalised distances from centroid of all pores

A pulsed MIG sample made with high heat input and interlayer temperature is compared to CMT sample made with low heat input and low interlayer temperature in Fig 13. As discussed earlier, CMT showed more uniform pore distribution as the pore centroid

normalised distance was smaller than compared to pulsed MIG sample for both small and large pores. Considerable variation in the average normalised distance was noted for pulsed MIG sample with high heat input and high interlayer temperature (P-HH-T2) for different pore sizes.
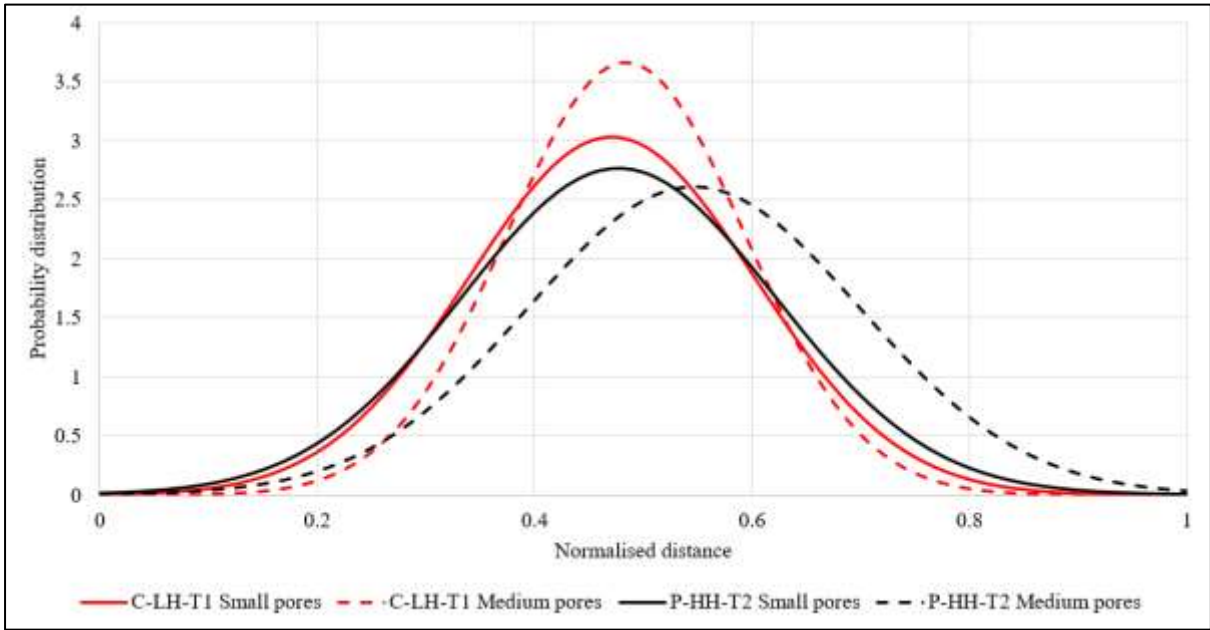
Fig 13 Normal distribution of pore normalised distances from centroid of all pores for two difference metal deposition conditions

3.6 Pore volume

The pore size and distribution can be directly correlated with the volume. In the CMT samples, the percentage of total pore volume occupied by small pores was higher than medium and large pores with small pores occupying more than 50% of the total pore volume (Fig 14a and b). Only exception to this finding was the sample with high heat input and 30 second interlayer dwell time (C-HH-t1) that showed 47.3% total pore volume (Fig 14a and b). Medium sized pores occupied total pore volume ranging between 31.5% and 44.7%. The maximum and minimum difference between volume fraction occupied by small and medium sized pores was 33.2% for sample C-HH-t2 and 2.55% for sample C-HH-t1 respectively. Also, large pores had a total volume fraction between 2.72% and 9.76% for the CMT samples.
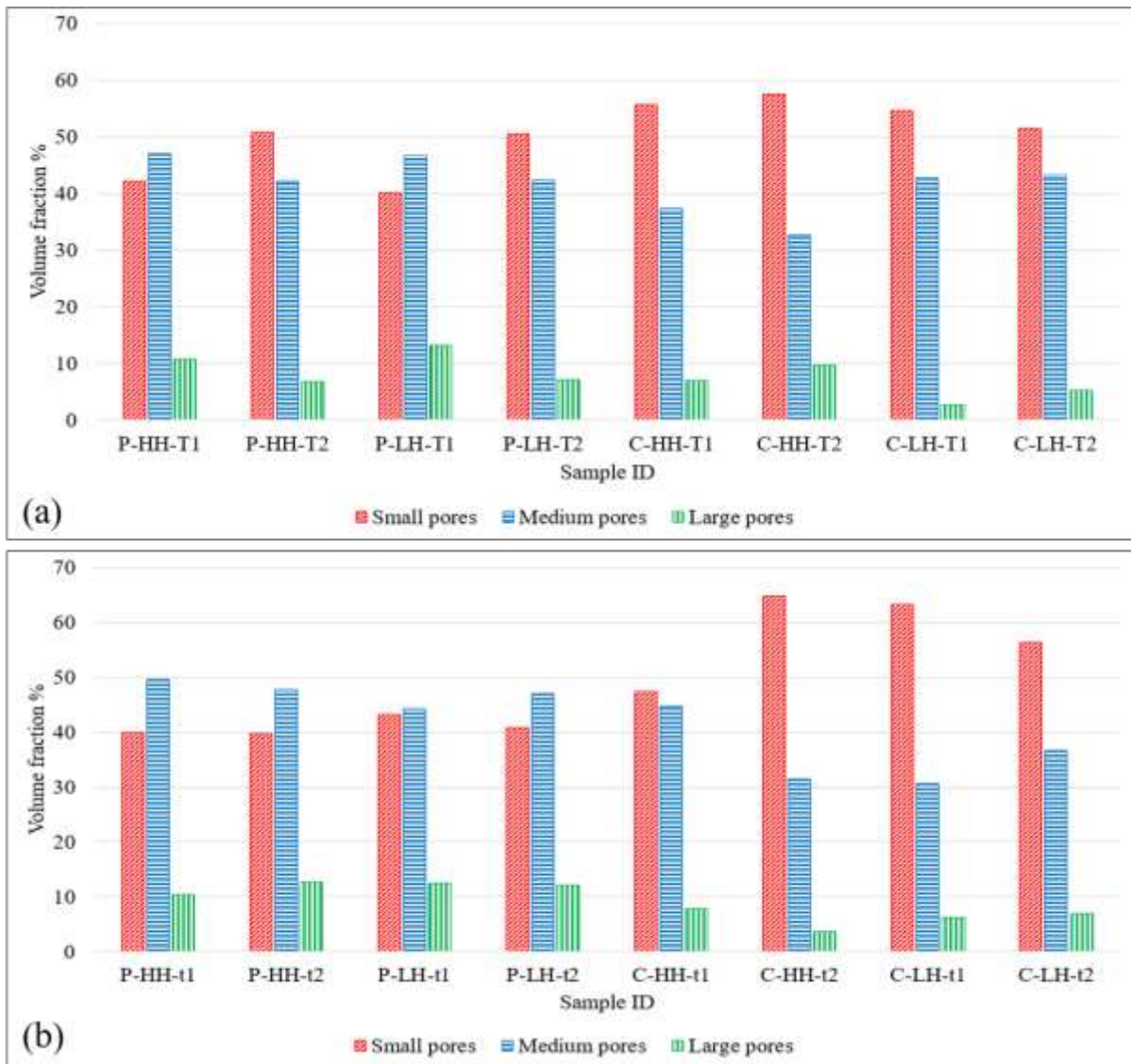
Fig 14 Volume fraction of different porosity size ranges in samples manufactured with (a) interlayer temperature control and (b) interlayer dwell time control

However, for samples manufactured with pulsed MIG, the results were markedly different (Fig 14a and b). Irrespective of the higher count of small pores, the total volume of medium size pores was higher than total volume of small size pores except for samples P-HH-T2 and P-LH-T2. The majority of the samples (six out of eight) revealed that medium size pores had higher total volume than the small size pores. Although the difference between the total volumes for the two pore sizes was small, it cannot be neglected. The difference between the total volume of medium and small pores was minimum for P-LH-t1 (0.91%) and maximum for P-HH-t1 (9.71%). Large pores showed total volume varying between 6.8% and 13.1% for pulsed MIG samples. Thus, compared with CMT samples, pulsed MIG samples showed higher total volume fraction of large sized pores. Average total volume fraction of large size pores was 6.1% for CMT samples while it was 10.8% for pulsed MIG samples.

3.7 Dissolved hydrogen

Two sets of samples namely DH1 and DH2 were selected that had the largest difference in porosity content between CMT and pulsed MIG samples (Table 6). The hydrogen measured

during the dissolved hydrogen test is the sum of hydrogen content released from pores after melting of test samples (hydrogen molecule) and dissolved hydrogen in a solid aluminium in atomic form. The term dissolved hydrogen in further discussion in this paper represents the hydrogen present/dissolved in solid solution of aluminium. Hence, absorbed hydrogen either forms pore or gets dissolved in solid aluminium which are termed and considered separately in further context of this paper.

It was observed that deposition of aluminium by pulsed MIG and CMT affects the total hydrogen content in the solidified volume as shown by Table 6. In both sets of samples, the total hydrogen content was comparable, however, the difference in total volume of pores between pulsed MIG and CMT samples revealed difference in the total hydrogen available per pore volume percentage. ==This content of detected hydrogen was significantly lower than the feed stock hydrogen content of ~ 7.5 ppm/100gm of metal. The reasons for differences in hydrogen content of wire and final build have been elaborated in the following section.==

Table 6 Comparison of hydrogen content obtained from dissolved hydrogen test in CMT and pulsed MIG samples

Set ID.	Process / technique	Sample ID	Pore volume fraction (%)	Detected hydrogen content (ppm)	Hydrogen content (ppm) / pore volume fraction (%) (ppm/volume %)
DH1	CMT	C-LH-T1	0.031	0.834	26.900
DH1	Pulsed MIG	P-LH-T1	0.152	0.993	6.530
DH2	CMT	C-LH-t2	0.038	1.020	26.840
DH2	Pulsed MIG	P-LH-t2	0.175	1.250	7.140

The total porosity volume fraction in the pulsed MIG samples were 4.9 and 4.6 times higher than that of CMT samples for set DH1 and DH2 respectively. Interestingly, for both sets, the total hydrogen content was found to be comparable. Comparing the presence of hydrogen available per pore volume fraction, it was clear that CMT samples revealed around 26 ppm of hydrogen per pore volume fraction, whereas pulsed MIG samples showed around only 7 ppm hydrogen for each pore volume fraction. Hence, hydrogen available per pore volume fraction in CMT samples was much more than that in pulsed MIG samples. This pointed towards the possibility of presence of dissolved hydrogen in aluminium solid solution. This has been further elaborated in discussion section.

4. Discussion

## 4.1 Interrelation between interlayer temperature and dwell time controls

As discussed in the section 2.2, manufacturing of sample Sets 1 and 2 were temperature controlled which were independent of the interlayer dwell time. As discussed by Wu et al. and Xiong et al. [24–26], temperature of the forming part increases as number of layers increases due to heat accumulation. Heat extraction by the substrate reduces temperature of the deposited layer and effect is prominent for initial few layers. As the distance between deposited layer and substrate increases heat extraction effect by the substrate diminishes increasing overall temperature of the forming part. Thus, high rate of heat extraction at the substrate rapidly reduced temperature of initially deposited layers. In order to maintain predefined interlayer temperature, successive layers were deposited with shorter time gap. Thus, interlayer dwell time was shorter for initial layers and successively increased for latter layers as heat accumulation increased in temperature based samples. Time taken by hot liquid metal to cool down to 100°C is less than to cool up to 50°C. Hence, during metal deposition, time taken by deposited metal to reach 100°C interlayer temperature is less than 50°C interlayer temperature which affects the interlayer dwell time of successive metal deposition in layers. At this point it should be noted that the interlayer dwell time for samples manufactured with 50°C interlayer temperature was longer than that for samples prepared with 100°C interlayer temperature. Thus, it can be deduced that samples manufactured with 100°C interlayer temperature were comparatively hotter all the time than the samples with 50°C interlayer temperature that offered more time to release heat to the surroundings.

Alternatively, all samples with fixed interlayer dwell times of 30 or 120 seconds were manufactured irrespective of the temperature of top layer. For each deposited layer, interlayer temperature was varying from low for the initial layers to high for higher number of layers due to heat accumulation effect discussed previously [25]. The shorter interlayer dwell time of 30 seconds induced increased heat accumulation than the longer interlayer dwell time of 120 seconds as the longer dwell time allowed more heat dissipation to substrate and surroundings. Samples prepared with 30 seconds interlayer dwell time were therefore hotter and had a higher interlayer temperature compared to the samples manufactured using 120 seconds interlayer dwell time. From the above discussion, it could be inferred that considering all other variables being constant, the samples manufactured with 50°C interlayer temperature were approximately comparable with samples manufactured using 120 seconds interlayer dwell time. Also, samples prepared using 100°C interlayer temperature could be comparable to samples manufactured with 30 seconds interlayer dwell time.

4.2 Effect of deposition technique and penetration

The penetration depth i.e. depth of re-melting of previously deposited layer is different between the CMT and pulse MIG processes due to the difference in metal transfer technique. The dip metal transfer, i.e. short circuit mode, lowers penetration as well as heat input in CMT [22] compared to pulsed MIG where metal deposition takes place usually by globular and spray transfer depending on the applied current. An illustration of the difference in penetration is shown in Fig 15. In the case of CMT, repeated cycles of arc on and off supported by electronically controlled forward and backward movement of feed wire ultimately reduces an arc energy and heat input [1,12] thus reducing the overall re-melting and penetration. The

pulsed MIG technique does not experience any retraction of wire and keeps the arc on all the time, although current pulsing reduces the overall arc energy. This can be observed by comparing Fig 3a with Fig 3b and Fig 3c with Fig 3d. where the heat input value reached almost zero during CMT, however, pulsed MIG samples showed positive non-zero minimum values confirming arc was on all the time.
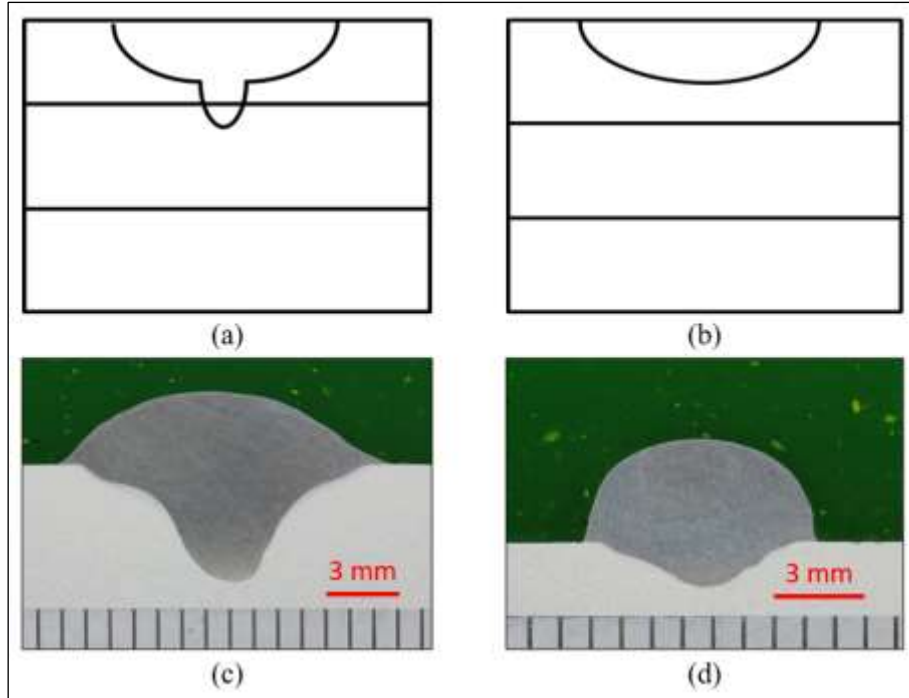
Fig 15 Effect of metal deposition technique on penetration in schematic and macro form (a) and (c) showing pulsed MIG and (b) and (d) represented CMT

From the schematic of the penetration, it can be argued that pores formed at the upper portion of a deposited layer were completely removed during deposition of a successive layer owing to the arc penetration effect. As a portion of layer gets melted, all the pores lying in the same area are naturally removed as a part of melting process. The same pores, hence hydrogen, are expected to be carried away into the newly formed and deposited liquid aluminium either by dissolution forming new pores, or by releasing to the atmosphere. This depends upon the local concentration of hydrogen and rate of gas absorption and evolution [15]. Considering the top layer in Fig 16, it is clear that both techniques formed pores at the upper portion of a layer. The pores close to top portion of a layer are within the penetration area and get removed while depositing the next layer. However, pores formed in the lower portion of a layer and at interlayer region remain untouched as can be clearly seen in Fig 16. This is because of limited penetration that could not reach the entire depth of a layer. Pronounced pore banding can be observed throughout the length of deposited layer in interlayer region in CMT as well as Pulsed MIG samples. As discussed earlier, pulsed MIG displays relatively hotter technique of metal deposition compared to CMT, hence there are more chances of hydrogen absorption due to higher operating temperature of arc and liquid aluminium in pulsed MIG technique [15]. A comparison of pulsed MIG and CMT with respect to effect of metal depositing parameters on hydrogen absorption and overall observations are summarised in Fig 17.
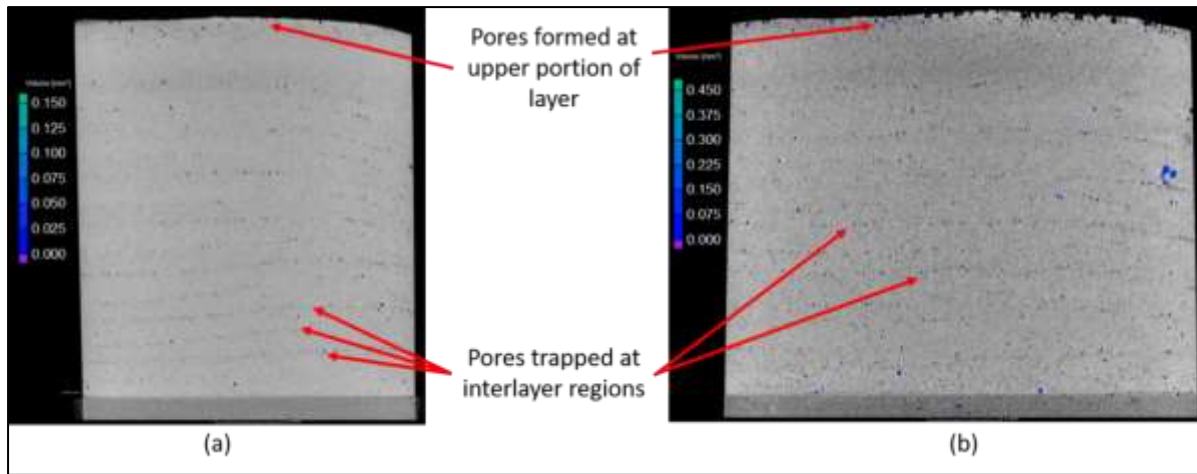
Fig 16 XCT image of porosity distribution shown in the longitudinal direction of samples prepared using (a) CMT technique and (b) pulsed MIG process
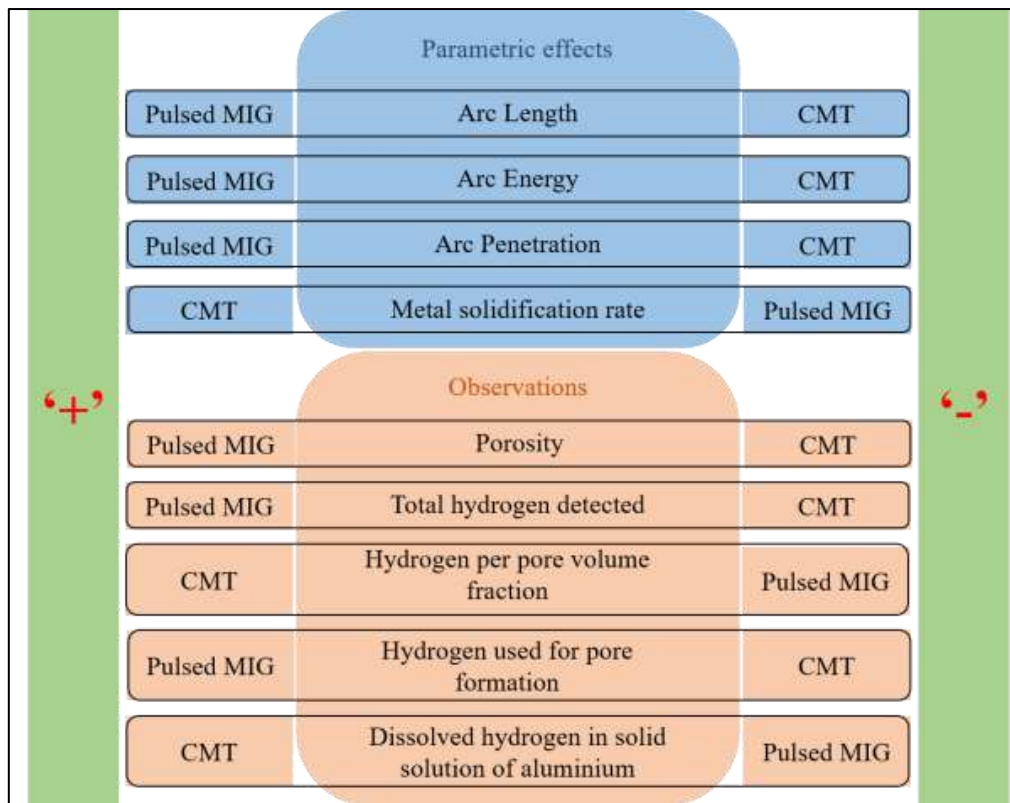

Fig 17 Effect of pulsed MIG and CMT metal deposition techniques on hydrogen absorption

Devletian and Wood [16] have pointed out that pore 'banding zones' is a common phenomenon in MIG welding of aluminium which resembles the solute banding in welds. It can be argued that pore banding observed in the samples shown in Fig 16, has a close relationship with banding zone formation in multi-pass welding due to the drastic rise in a solidification rate at solid-liquid interface that results in formation of a porosity entrapped zone. Thus, periodic variation in solidification rate is found to have a major influence on banding formation. Porosity formation in solid state referred to as secondary porosity could be another

possible reason for increased pores at interlayer regions that can be formed due to subsequent reheating at/or near solidus temperature which is the strongly the case in WAAM [16].

4.3 Absorbed hydrogen

Hydrogen bubble formation in liquid aluminium will take place only when the hydrogen concentration in liquid at liquid-solid interface reaches the maximum solubility limit of hydrogen in solid aluminium [27]. Also, in MIG operations, hydrogen in liquid metal is absorbed up to its maximum solubility limit at the central part of arc and distributed to other parts by convection. Solidification morphology, solubility considerations, hydrogen pressure, nucleation and growth kinetics determine hydrogen bubble formation and the size, shape and distribution of porosity in solidified metal [16].

From Table 6 it was clear that relatively higher percentage of hydrogen was available in CMT processed samples than pulsed MIG samples for pore formation. Porosity volume fraction was 4.9 and 4.6 times (sets DH1 and DH2 respectively) higher in pulsed MIG samples compared to CMT, however, hydrogen available per pore volume fraction was higher for CMT samples than pulsed MIG by almost the same factor (4.1 and 3.7 for DH1 and DH2 respectively). This is because of the difference in the porosity volume fraction in two types of samples against relatively similar amount of available hydrogen. Considering all the pores present in samples were filled with hydrogen gas and no pores were formed due to solidification shrinkage without hydrogen, comparatively more hydrogen should remain dissolved in solid aluminium.

The values of hydrogen detected in test are given in Table 7 (refer annexure for detailed calculations). The results are in close agreement with results reported by Devletian and Wood [16] that showed solid solubility of 1.2 ml / 100 gm for 5183 alloy composition. The expected content total hydrogen per 100 g of samples is higher in pulsed MIG than CMT samples. It can be concluded that total hydrogen pick up from wire and atmosphere in pulsed MIG was more than CMT samples due to the reasons discussed. Hydrogen pick up from wire in pulsed MIG and CMT can be considered equal as the same wire spool was used for manufacturing of the samples. Hotter liquid metal is prone to hydrogen absorption into the molten pool. Hence, it can be argued that pulsed MIG samples picked up greater percentage of hydrogen from the wire than CMT. Thus, as observed and discussed earlier, it can be confirmed from Table 7 that more hydrogen was available for pore formation in pulsed MIG samples than CMT samples. Increased dissolved hydrogen combined with slower cooling rate led to higher volume fraction of porosity in pulsed MIG. It suggests pulsed MIG metal deposition technique eases pore coalescence in aluminium [16] compared to CMT process. It might be correlated to the availability of larger liquid metal pool [15] in pulsed MIG than CMT. Also, this might aid easier hydrogen movement for coalescence of atomic hydrogen to form a hydrogen molecule, hence, hydrogen gas responsible for pore formation that could not escape out due to solid formation.

As discussed in the previous section, the detected hydrogen in build samples was much lower compared to hydrogen content in feed stock material. Following factor may influence the observed difference between hydrogen contents; i) as mentioned in experimental section, the hydrogen content detected in wire can be skewed because of organic matter which gets retained in the surface irregularities/roughness features even after cleaning the wire [18,19]. ii) The argon used in current study was 99.998% pure indicating that it would have other gaseous

Table 7 Comparison of total hydrogen content, hydrogen in pores and dissolved hydrogen obtained from dissolved hydrogen test in samples prepared using CMT and pulsed MIG (refer Annexure)

Set ID	Samples ID	Total hydrogen in samples of 100 g (ml)	Percentage of hydrogen forming pores	Percentage of hydrogen in solid solution
DH1	C-LH-T1	0.934	1.220	98.780
	P-LH-T1	1.112	5.060	94.940
DH2	C-LH-t2	1.142	1.250	98.750
	P-LH-t2	1.400	4.480	95.520

In both sets (DH1 and DH2), the volume of hydrogen in the pores was greater for pulsed MIG samples than CMT. Considering the rest of the hydrogen (apart from being entrapped in the pores), pulsed MIG samples showed around 95% dissolved hydrogen, whereas, CMT samples showed more than 98.75%. For all these calculations, the total hydrogen detected during the testing was considered to be present either in the pores or at lattice imperfections in atomic form in a dissolved state. From Table 6 and Table 7 it can be argued that pulsed MIG samples absorbed higher percentage of hydrogen leading to higher porosity than the CMT samples. As a result more hydrogen was consumed for pore formation in pulsed MIG leaving behind lower fraction of hydrogen in dissolved state. Hence, although CMT samples absorbed relatively lesser hydrogen from the atmosphere and formed fewer pores than pulsed MIG samples, CMT showed higher dissolved hydrogen due to number of reasons as discussed earlier.

4.4 Arc length effect

Comparing the two metal deposition techniques, pulsed MIG maintains a relatively constant arc length throughout the metal deposition process, however, for CMT the arc length continuously changes from maximum to zero due to short circuiting mode. Thus, liquid aluminium globules and/or small droplets in a spray form are exposed to the contaminations and surrounding atmosphere for relatively longer time in pulsed MIG than CMT. This allows longer time for liquid aluminium to absorb hydrogen from contamination and from shielding gas, if any [15]. Also, the surface area of the globules and spray droplets formed from pulsed MIG must have been considerably higher than a droplet that formed and transferred to molten pool during CMT. At this point it can be argued that the pulsed MIG samples absorbed more hydrogen than the CMT samples due to greater exposure time to the contaminants and relatively higher surface area of deposited liquid aluminium. The fact reflected in Table 4 as total volume fraction of the pore in pulsed MIG samples was greater than CMT samples for all the cases considered.

4.5 Cooling and solidification rate effects

It is well accepted that hydrogen in aluminium can be found at pore sites as well as in solid solution at lattice imperfections such as grain boundaries, dislocations, impurities etc.

[29]. During liquid metal solidification pores are formed at the solidification front due to rejection of dissolved hydrogen [14]. The process of rejection of dissolved gas from liquid metal is time dependent. If the solidification rate is high, there are increased chances of dissolved hydrogen remaining entrapped in the solid metal. For the processes used in this study, CMT allows metal to solidify at a faster rate due to its peculiar technique of metal deposition [30] compared to pulsed MIG. Hence, it could be deduced that samples made with CMT had more chances of retaining dissolved hydrogen in the solid aluminium than those made with pulsed MIG. In line with this, dissolved hydrogen in the molten aluminium is expected to give rise to pore formation as it solidifies, however, pulsed MIG samples showed more total pore volume than CMT samples as discussed in earlier and from Table 4. In the case of pulsed MIG processing, the relatively low solidification rate increases chances of hydrogen pick up in the molten metal [15]. This could be one of the reasons for higher total hydrogen content in pulsed MIG samples.

According to Devletian and Wood [16], solidification mechanism in MIG welding showed substantial influence on the pore formation and distribution. Interstices between growing dendrites provide regions for hydrogen bubble formation, however, its detachment and floatation into available liquid aluminium depends upon the size and shape of the gaps between forming dendrites. At faster cooling rate, trapped hydrogen bubbles cannot grow with similar rate as that of progressing closely packed cells, hence, they remain entrapped between the forming cells and find restriction to detach and grow [31]. For slower cooling rate, dendrites are widely spaced providing relatively increased area for pores that take the available space [16]. This could be another probable reason for the formation of large sized pores in pulsed MIG samples than CMT samples.

4.6 Secondary heat effects

During metal deposition in layer format, the temperature of a deposit is raised. The degree of temperature rise at a point in a deposit depends upon its distance from the top depositing layer, thermal conductivity of alloy composition and arc energy. The temperature distribution during metal deposition has been discussed by Xiong et al. [25] and [26]. Temperature of the layer on which a new layer is deposited is usually raised above the melting temperature (penetration effect confirms the same) of that metal and subsequent layers above recrystallization temperature.

At such a high temperature concentration of vacancies becomes significant and influences hydrogen diffusion [29,32] due to large binding energy between hydrogen atom and vacancy. Hashimoto and Kino [29] proved the dependency of the hydrogen diffusion on the concentration of vacancies and concentration of dissolved hydrogen in aluminium at high and low temperatures. In pulsed MIG samples, due to comparatively higher arc energy, penetration and forced vacancy diffusion, hydrogen diffusion; could have been comparatively more than the CMT samples. Rapid solidification, less penetration and less arc energy in CMT could have less influence on hydrogen diffusion compared to pulsed MIG. Thus, increased movement of hydrogen along with vacancies may have formed clusters [14] that grew as a large sized pores in pulsed MIG samples. The fact explained the presence of relatively large size pores and the increased volume fraction of large size pores in pulsed MIG samples than in CMT samples (Fig 5a, Fig 5b, Fig 14a and Fig 14b).

Results of section 3.2.2 and 3.2.3 illustrated pulsed MIG samples showing higher total pore volume for low heat input and low interlayer temperature control methods. Thus, reduced total pore volume for the samples with high heat input and high interlayer temperature condition. The results are in agreement with the results discussed by Derekar et al. [33]. However, CMT samples showed higher total pore volume for high heat input and high interlayer temperature controls and low total pore volume for low heat input and low interlayer temperature. The contradictory results indicate that pore formation due to solidification and from coalescence have close relation with the heat content in the deposit. It appears from the results that high heat input and high interlayer temperature conditions in pulsed MIG deposition mode are high enough to provide sufficient heat required for hydrogen coalescence which supported the pore formation and escape of formed pores. However, low heat input and low interlayer temperature condition in CMT cannot raise temperature high enough to aid hydrogen coalescence and further escape of pores. Increased pore formation conditions in both processes i.e. low heat input low interlayer temperature for pulsed MIG and high heat input high interlayer temperature in CMT, provide sufficient heat for hydrogen formation and hydrogen coalescence, however, the heat is not sufficiently high for releasing the hydrogen in the form of pores. It is worth mentioning again that compared to pulsed MIG, CMT is colder process. Thus heat input can be seen to affect hydrogen dissolution and coalescence in both processes but further analysis is required to quantify these results and the postulation.

4.7 Statistical analysis

A statistical analysis was performed using analysis-of-variance (ANOVA) in order to verify the differences in porosity diameter occurred in different samples manufacturing using different metal deposition conditions. For analysis purposes, the p-values obtained from ANOVA were considered. Typically, the null hypothesis assumes that there is no difference in the porosity diameters between samples. Considering a 95% confidence, if the p-value between samples is less than 0.05, the null hypothesis is false, suggesting there is a difference in porosity diameters. Table 8 to Table 10 compares p-values of different sample combinations. From Table 8, no samples revealed p-value less than 0.05 indicating that there is no statistically significant difference in the porosity diameters of the samples produced using a pulsed MIG process. However, for a CMT process, the variable inputs have a significant influence on the porosity diameter. Within the CMT conditions in Table 8, it is evident that heat input develops statistically significant differences in the diameters; however, the samples with variable interlayer temperature and interlayer dwell time only show marginal differences. With different interlayer temperatures at low heat inputs, the confidence of null hypothesis being false is 86.13%, which lowers down to 64.09% in case of high heat input. This is also the case in variable interlayer dwell time that indirectly affects interlayer temperature as explained subsection 4.1.

Table 8 Comparison of p-values obtained for interlayer temperature, interlayer dwell time and heat input sample combinations within respective CMT and pulsed MIG deposition

Comparison	CMT		Pulsed MIG	
	Sample IDs	p-values	Sample IDs	p-values
Interlayer temperature	C-HH-T1 C-HH-T2	0.3591	P-HH-T1 P-HH-T2	0.552
	C-LH-T1 C-LH-T2	0.1387	P-LH-T1 P-LH-T2	0.7614

Condition	Sample ID	p-value	Sample ID	p-value
Interlayer dwell time	C-HH-t1 C-HH-t2	0.359	P-HH-t1 P-HH-t2	0.625
	C-LH-t1 C-LH-t2	0.2247	P-LH-t1 P-LH-t2	0.6318
Heat input	C-HH-T1 C-LH-T1	1.1×10^{-38}	P-HH-T1 P-LH-T1	0.2662
	C-HH-T2 C-LH-T2	4.49×10^{-40}	P-HH-T2 P-LH-T2	0.3865
	C-HH-t1 C-LH-t1	1.37×10^{-75}	P-HH-t1 P-LH-t1	0.6669
	C-HH-t2 C-LH-t2	2.93×10^{-44}	P-HH-t2 P-LH-t2	0.4657

When the comparison was made between the samples from CMT and pulsed MIG processes in Table 9, low heat input samples proved hypothesis false with p-values much lower than 0.05. This suggests that pore diameters in the samples of CMT and pulsed processes for low heat input conditions affects more than high heat input. Although, statistical results indicated that pores produced by high heat input condition in CMT and pulsed MIG were similar, the confidence of hypothesis being true was not strong.

Table 9 Comparison of p-values obtained for CMT and pulsed MIG processed sample combinations for considered metal deposition parameters

Condition		Sample ID	p-values
High heat input	Interlayer temperature	C-HH-T1 P-HH-T1	0.3216
		C-HH-T2 P-HH-T2	0.246
	Interlayer dwell time	C-HH-t1 P-HH-t1	0.3871
		C-HH-t2 P-HH-t2	0.1172
Low heat input	Interlayer temperature	C-LH-T1 P-LH-T1	1.23×10^{-37}
		C-LH-T2 P-LH-T2	3.69×10^{-38}
	Interlayer dwell time	C-LH-t1 P-LH-t1	4.57×10^{-91}
		C-LH-t2 P-LH-t2	5.11×10^{-86}

From another chosen combinations as detailed in Table 10, sample with hot deposition conditions such as pulsed MIG-high heat input-high interlayer temperature was compared with sample produced with relatively cold conditions such as CMT-low heat input-low interlayer temperature and results showed that extreme heat conditions had significant effects on pore diameters formed which was also evident from results section. In another condition with comparable heats (samples P-LH-T1 and C-HH-T2) was also confirmed CMT and pulsed MIG produced different sized pores. The interrelation between interlayer temperature and interlayer

dwell time based deposition techniques was statistically studied considering its effect on pore diameters. In line with discussion in section 4.1, samples with 50 and 100°C interlayer temperatures were compared with samples having 120 and 30 seconds of interlayer dwell times respectively. CMT low heat input condition showed that samples were significantly different. Although statistically not proved, the condition was not appreciably different in case of high heat input samples which showed confidence of null hypothesis being false was around 90%. All pulsed MIG samples combinations in the similar category showed mathematically invariant, however, a pattern can be drawn from the results. High heat conditions such as high heat input and interlayer temperature (as well as short interlayer dwell time) samples and low heat conditions such as low heat input and interlayer temperature (and long interlayer dwell time) samples revealed statistically no variations in pore diameters. However, in reversed conditions, high heat input with low interlayer temperature (and long interlayer dwell time) and low heat input with high interlayer temperature (and short interlayer dwell time), statistically samples showed similar pore diameters but p-values were around 0.27 indicating that 83% of confidence being samples showed different pore diameters. The results are in coordination with discussion made in subsection 4.1, 4.2 4.5 and 4.6.

Table 10 Comparison of p-values obtained for different sample combinations for considered metal deposition parameters

Condition		Sample IDs	p-values
Extreme condition of heat content		P-HH-T2 C-LH-T1	1.44×10^{-30}
Comparable condition of heat content		P-LH-T1 C-HH-T2	0.0336
Comparable condition of temperature and time based samples	CMT	C-HH-T1 C-HH-t2	0.1029
		C-HH-T2 C-HH-t1	0.092
		C-LH-T1 C-LH-t2	1.5×10^{-12}
		C-LH-T2 C-LH-t1	6.27×10^{-29}
	Pulsed MIG	P-HH-T1 P-HH-t2	0.2719
		P-HH-T2 P-HH-t1	0.6474
		P-LH-T1 P-LH-t2	0.709
		P-LH-T2 P-LH-t1	0.2708

5. Conclusions

1. Pulsed MIG always showed higher pore content than CMT. For both processes, majority of pores were in small size range (pore diameter 0.11 – 0.20 mm). However, pulsed MIG showed higher percentage of medium (0.21 – 0.30 mm) and large size (> 0.31 mm) pores than CMT. Irrespective of majority of the small pores, pulsed MIG

showed higher pore volume for medium sized pores (0.21 – 0.3 mm), however, small size pore volume was greater in CMT.

2. Pulsed MIG picked up more hydrogen than CMT because higher arc energy resulted in a larger, hotter and slower cooling melt pool which had greater susceptible to hydrogen absorption.

3. Pulsed MIG retained a lower percentage of absorbed hydrogen in solid solution than CMT. The remaining hydrogen was consumed in pore formation during the solidification phase.

4. Pulsed MIG had higher total pore volume fraction for process conditions of low heat input, low interlayer temperature and longer dwell time control methods than high heat input, high interlayer temperature and shorter dwell time. The reverse was true for CMT.

Annexure - A

Dissolved hydrogen calculations for sample C-LH-T2 –

(1) Total volume of the sample pore measurement by X-CT scan = 1440 mm^3

Mass of the sample considered can be calculated as –

Mass = density x volume

$= 2.7 \times 10^{-3}$ (g/mm^3) x 1440 mm^3

= 3.888 g

(2) Total volume of the pores found in 1440 mm^3 (3.888 g) of samples volume = 0.44 mm^3

(3) Weight of the samples tested for dissolved hydrogen = 0.402 g

Thus, corresponding volume of the pores in samples of weight 0.402 g can be calculated as –

= 0.402 (g) x 0.44 (mm^3) / 3.888 (g) = 0.04549 mm^3

(4) Total hydrogen detected after dissolved hydrogen test 0.834 ppm

ppm to ml conversion can be as follows –

1 ppm = 1.12 (ml) / 100 (g)

Thus, 0.834 ppm are –

= 0.834 (ppm) x 1.12 (ml / 100 g) / 1 (ppm) = 0.93408 ml / 100 g

Hence, 0.93408 ml of hydrogen per 100 g of metal.

(5) Weight of the samples for dissolved hydrogen test was 0.402 g.

Thus, total hydrogen for 0.402 g of metal can be calculated as –

= 0.93408 (ml) x 0.402 (g) / 100 (g) = 0.003755 ml

Hence, 0.402 g of tested samples showed 0.003755 ml (375.5×10^{-5} ml) of total detected dissolved hydrogen.

(6) From point (3), we know that 0.402 g of samples showed 0.04549 mm^3 of pore volume. Here we are assuming that all the pores are completely filled with hydrogen. Therefore, converting pore volume from mm^3 to ml, we get –

= 0.04549 (mm^3) = 4.549 x 10^{-5} (ml)

Hence, in a sample of weight 0.402 g with 0.04549 mm^3 of pore showed 4.549 x 10^{-5} ml of hydrogen.

(7) From point (5) we know that total hydrogen in sample was 375.5 x 10^{-5} ml. From point (6) it was clear that hydrogen in the pore was 4.549 x 10^{-5} ml. Thus, dissolved hydrogen ca ne calculated as –

= (375.5 – 4.549) x 10^{-5}

= 370.951 x 10^{-5} ml

Dissolved hydrogen in the sample was 0.00370951 ml (370.951 x 10^{-5} ml)

(8) Percentage of dissolved hydrogen with respect to total hydrogen in sample –

= (370.951 x 10^{-5}) / (375.5 x 10^{-5}) x 100

= 98.78 %

Thus, samples CBJ showed 98.78% of dissolved hydrogen and 1.22% of hydrogen in pores.

Dissolved hydrogen values for other samples after following similar calculations are summarised in Table A.

Table A Details of dissolved hydrogen values samples wise

Samples ID	Weight of samples consumed in dissolved hydrogen test (g)	Total detected hydrogen in sample (ml)	Expected total hydrogen in samples of 100 g (ml)	Volume of hydrogen at pores (%)	Dissolved hydrogen volume in solid sample (%)
C-LH-T1	0.402	0.003755	0.934	1.22	98.78
P-LH-T1	0.5659	0.006293	1.112	5.06	94.94
C-LH-t2	0.2899	0.003311	1.142	1.25	98.75
P-LH-t2	0.5015	0.007021	1.4	4.48	95.52

Conflict of Interest: The authors declare that they have no conflict of interest.

References

[1]   K.S. Derekar, A review of wire arc additive manufacturing and advances in wire arc additive manufacturing of aluminium, Mater Sci Technol (United Kingdom). 34 (2018) 895–916. doi:10.1080/02670836.2018.1455012.

[2]   F. Martina, J. Mehnen, S.W. Williams, P. Colegrove, F. Wang, Investigation of the

benefits of plasma deposition for the additive layer manufacture of Ti-6Al-4V, J Mater Process Technol. 212 (2012) 1377–1386. doi:10.1016/j.jmatprotec.2012.02.002.

[3]   S.W. Williams, F. Martina, A.C. Addison, J. Ding, G. Pardal, P. Colegrove, Wire + Arc Additive Manufacturing, Mater Sci Technol. 32 (2016) 641–647. doi:10.1179/1743284715Y.0000000073.

[4]   D. Yang, C. He, G. Zhang, Forming characteristics of thin-wall steel parts by double electrode GMAW based additive manufacturing, J Mater Process Technol. 227 (2016) 153–160. doi:10.1016/j.jmatprotec.2015.08.021.

[5]   C. Zhang, Y. Li, M. Gao, X. Zeng, Wire arc additive manufacturing of Al-6Mg alloy using variable polarity cold metal transfer arc as power source, Mater Sci Eng A. 711 (2018) 415–423. doi:10.1016/j.msea.2017.11.084.

[6]   X. Fang, L. Zhang, G. Chen, X. Dang, K. Huang, L. Wang, B. Lu, Correlations between microstructure characteristics and mechanical properties in 5183 aluminium alloy fabricated by wire-arc additive manufacturing with different arc modes, Materials (Basel). 11 (2018). doi:10.3390/ma11112075.

[7]   J. Gu, X. Wang, J. Bai, J. Ding, S. Williams, Y. Zhai, K. Liu, Deformation microstructures and strengthening mechanisms for the wire+arc additively manufactured Al-Mg4.5Mn alloy with inter-layer rolling, Mater Sci Eng A. 712 (2018) 292–301. doi:10.1016/j.msea.2017.11.113.

[8]   J. Gu, J. Ding, S.W. Williams, H. Gu, J. Bai, Y. Zhai, P. Ma, The strengthening effect of inter-layer cold working and post-deposition heat treatment on the additively manufactured Al-6.3Cu alloy, Mater Sci Eng A. 651 (2016) 18–26. doi:10.1016/j.msea.2015.10.101.

[9]   J. Gu, B. Cong, J. Ding, S.W. Williams, Y. Zhai, Wire+Arc Additive Manufacturing of Aluminium, in: Proc 25th Annu Int Solid Free Fabr Symp, Austin, Texas, 2014: pp. 4–6.

[10]   Z. Qi, B. Cong, B. Qi, H. Sun, G. Zhao, J. Ding, Microstructure and mechanical properties of double-wire + arc additively manufactured Al-Cu-Mg alloys, J Mater Process Technol. 255 (2018) 347–353. doi:10.1016/j.jmatprotec.2017.12.019.

[11]   J. Gu, J. Ding, S.W. Williams, H. Gu, P. Ma, Y. Zhai, The effect of inter-layer cold working and post-deposition heat treatment on porosity in additively manufactured aluminum alloys, J Mater Process Technol. 230 (2016) 26–34. doi:10.1016/j.jmatprotec.2015.11.006.

[12]   B. Cong, J. Ding, S. Williams, Effect of arc mode in cold metal transfer process on porosity of additively manufactured Al-6.3%Cu alloy, Int J Adv Manuf Technol. 76 (2014) 1593–1606. doi:10.1007/s00170-014-6346-x.

[13]   A. Horgar, H. Fostervoll, B. Nyhus, X. Ren, M. Eriksson, O.M. Akselsen, Additive manufacturing using WAAM with AA5183 wire, J Mater Process Technol. 259 (2018) 68–74. doi:10.1016/j.jmatprotec.2018.04.014.

[14]   P. Yousefian, M. Tiryakioğlu, Pore Formation During Solidification of Aluminum: Reconciliation of Experimental Observations, Modeling Assumptions, and Classical Nucleation Theory, Metall Mater Trans A Phys Metall Mater Sci. 49 (2018) 563–575. doi:10.1007/s11661-017-4438-6.

[15]   G. Mathers, The welding of aluminium and its alloys, Woodhead publishing limited,

Cambridge England, Cambridge UK, 2002. doi:10.1533/9781855737631.1.

[16] J. Devletian, W. Wood, Factors affecting porosity in aluminum welds - A review, Weld Res Counc. 290 (1983) 1–18.

[17] H. Geng, J. Li, J. Xiong, X. Lin, Optimisation of interpass temperature and heat input for wire and arc additive manufacturing 5A06 aluminium alloy, Sci Technol Weld Join. 22 (2017) 472–483. doi:10.1080/13621718.2016.1259031.

[18] E.M. Ryan, T.J. Sabin, J.F. Watts, M.J. Whiting, The influence of build parameters and wire batch on porosity of wire and arc additive manufactured aluminium alloy 2319, J Mater Process Tech. 262 (2018) 577–584. doi:10.1016/j.jmatprotec.2018.07.030.

[19] J.L. Gu, J.L. Ding, B.Q. Cong, J. Bai, H.M. Gu, S.W. Williams, Y.C. Zhai, The Influence of Wire Properties on the Quality and Performance of Wire+Arc Additive Manufactured Aluminium Parts, Adv Mater Res. 1081 (2014) 210–214. doi:10.4028/www.scientific.net/AMR.1081.210.

[20] B. Cong, Z. Qi, B. Qi, H. Sun, G. Zhao, J. Ding, A Comparative Study of Additively Manufactured Thin Wall and Block Structure with Al-6.3%Cu Alloy Using Cold Metal Transfer Process, Appl Sci. 7 (2017) 275. doi:10.3390/app7030275.

[21] S. Kou, Metallurgy Second Edition Welding Metallurgy, 2003. doi:10.1016/j.theochem.2007.07.017.

[22] B. Cong, R. Ouyang, B. Qi, J. Ding, Influence of Cold Metal Transfer Process and Its Heat Input on Weld Bead Geometry and Porosity of Aluminum-Copper Alloy Welds, Rare Met Mater Eng. 45 (2016) 606–611. doi:10.1016/S1875-5372(16)30080-7.

[23] Y.X. Gao, J.Z. Yi, P.D. Lee, T.C. Lindley, The effect of porosity on the fatigue life of cast aluminium-silicon alloys, Fatigue Fract Eng Mater Struct. 27 (2004) 559–570. doi:https://doi.org/10.1111/j.1460-2695.2004.00780.x.

[24] B. Wu, D. Ding, Z. Pan, D. Cuiuri, H. Li, J. Han, Z. Fei, Effects of heat accumulation on the arc characteristics and metal transfer behavior in Wire Arc Additive Manufacturing of Ti6Al4V, J Mater Process Technol. 250 (2017) 304–312. doi:10.1016/j.jmatprotec.2017.07.037.

[25] J. Xiong, Y. Lei, R. Li, Finite element analysis and experimental validation of thermal behavior for thin-walled parts in GMAW-based additive manufacturing with various substrate preheating temperatures, Appl Therm Eng. 126 (2017) 43–52. doi:10.1016/j.applthermaleng.2017.07.168.

[26] J. Xiong, R. Li, Y. Lei, H. Chen, Heat propagation of circular thin-walled parts fabricated in additive manufacturing using gas metal arc welding, J Mater Process Technol. 251 (2018) 12–19. doi:10.1016/j.jmatprotec.2017.08.007.

[27] G. Grigorenko, Formation of pores in welds, Avtom Svarka. 10 (1970) 13–17.

[28] M. Hasegawa, Ellingham Diagram, Elsevier Ltd., 2014. doi:10.1016/B978-0-08-096986-2.00032-1.

[29] E. Hashimoto, T. Kino, Hydrogen diffusion in aluminium at high temperatures, J Phys F Met Phys. 13 (1983) 1157–1165. doi:10.1088/0305-4608/13/6/013.

[30] P. Wang, S. Hu, J. Shen, Y. Liang, Characterization the contribution and limitation of the characteristic processing parameters in cold metal transfer deposition of an Al alloy, J Mater Process Technol. 245 (2017) 122–133.

doi:10.1016/j.jmatprotec.2017.02.019.

[31] B. Chalmers, Principles of Solidification, in: Appl Solid State Phys, Springer, Boston, MA, 1970: pp. 161–170. doi:10.1007/978-1-4684-1854-5_5.

[32] S. Llnderoth, Hydrogen diffusivity in aluminium, Philos Mag Lett. 57 (1988) 229–234. doi:10.1080/09500838808214712.

[33] K. Derekar, J. Lawrence, G. Melton, A. Addison, X. Zhang, L. Xu, Influence of Interpass Temperature on Wire Arc Additive Manufacturing (WAAM) of Aluminium Alloy Components, in: MATEC Web Conf, 2019: p. 05001. doi:10.1051/matecconf/201926905001.
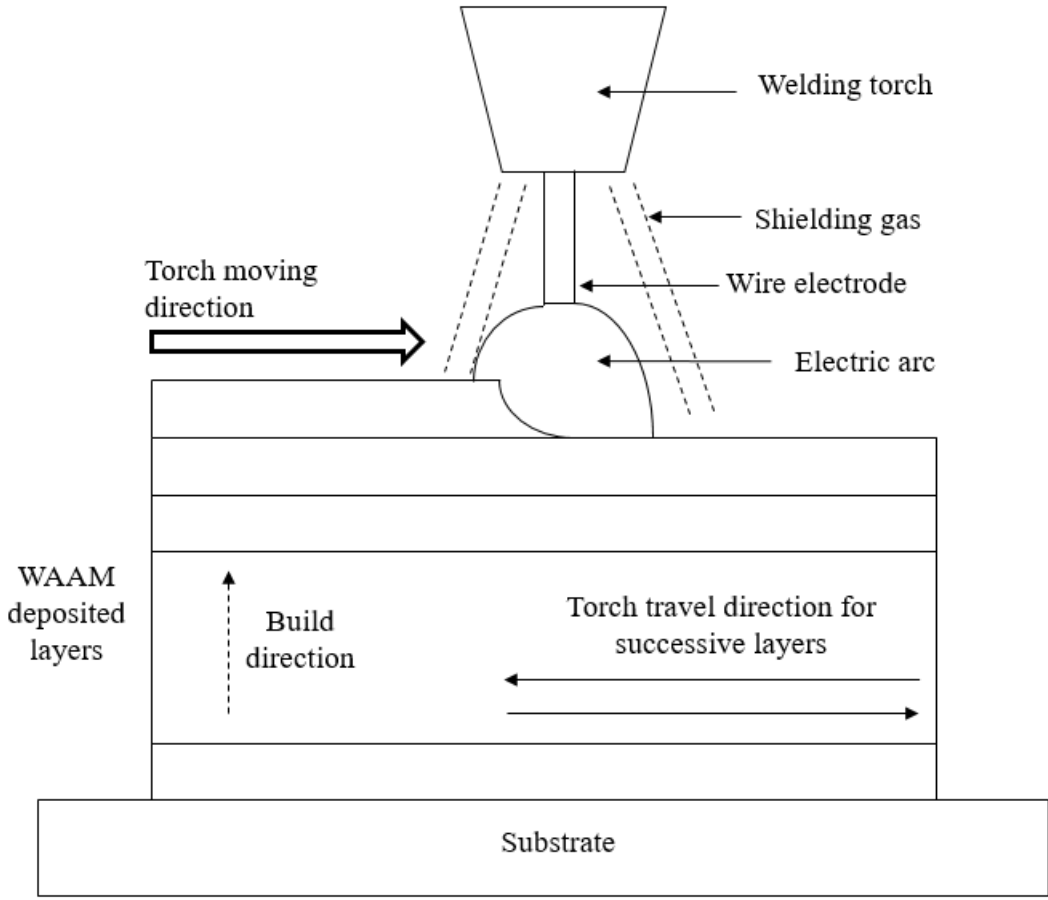
Fig 1 Schematic of WAAM deposition using gas metal arc technique

1

2

3

4

5

6

7

8

9
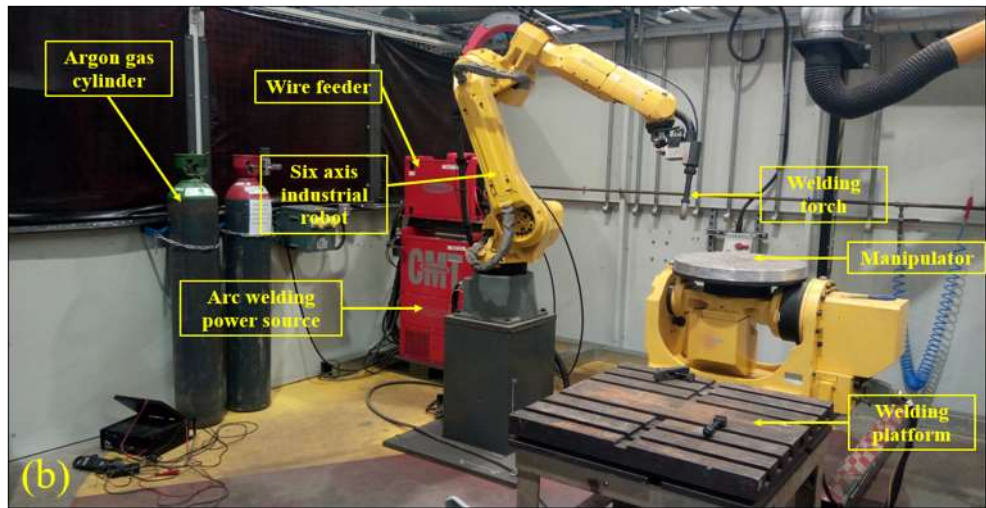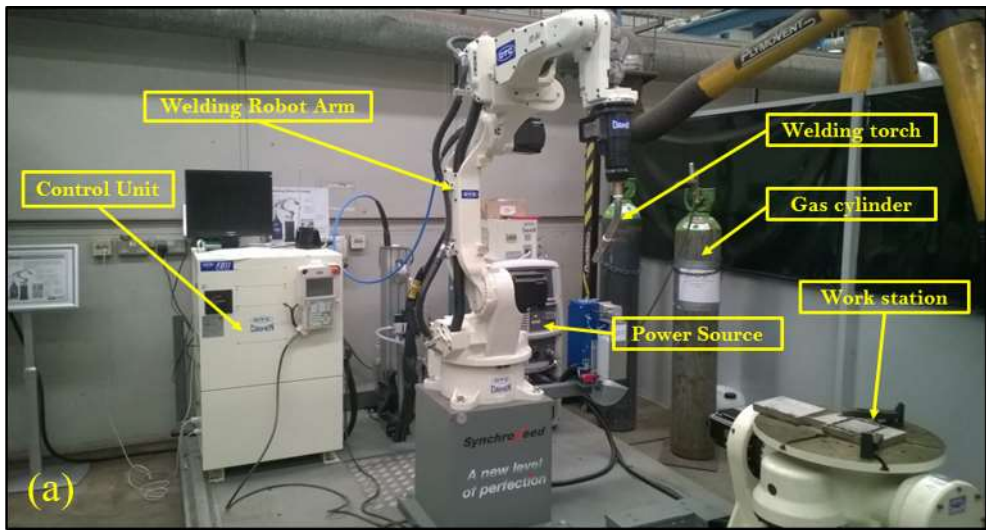
10

Fig 2 Welding robot (a) OTC Daihen Synchrofeed welding robot for pulsed metal inert gas (MIG) technique (b) Fronius CMT-Fanuc work station for cold

13
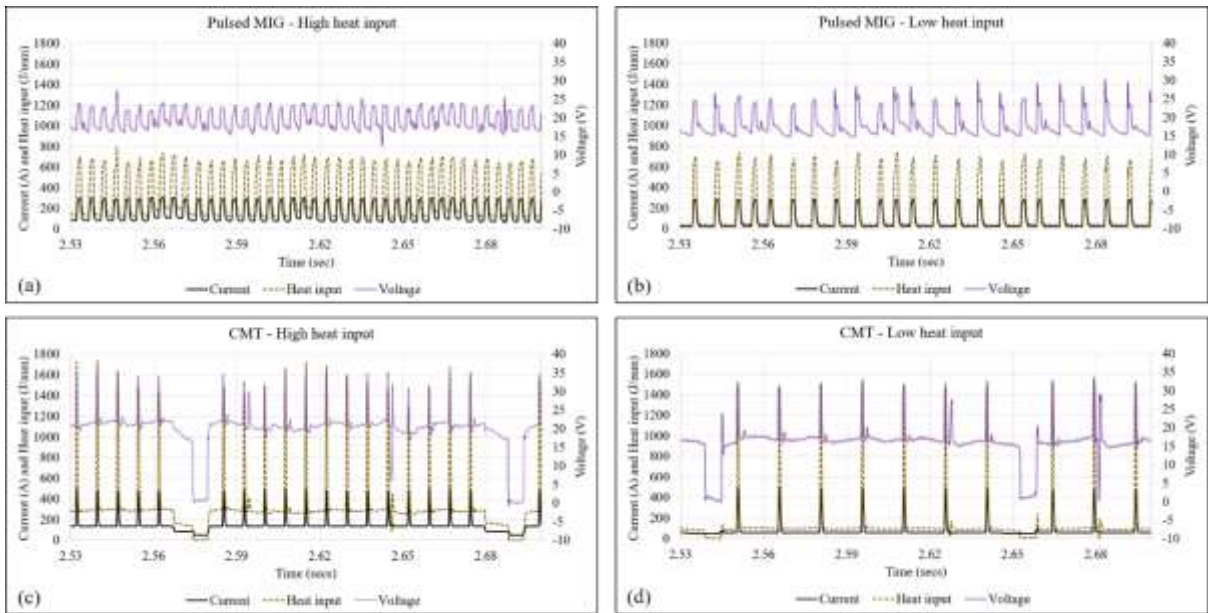
14

15

16

1

2

3

4

5

6

7

8

9

Fig 3 Current, voltage and heat input variations using (a) pulsed MIG high heat input (b) pulsed MIG low heat input (c) CMT high heat input and (d) CMT low heat input
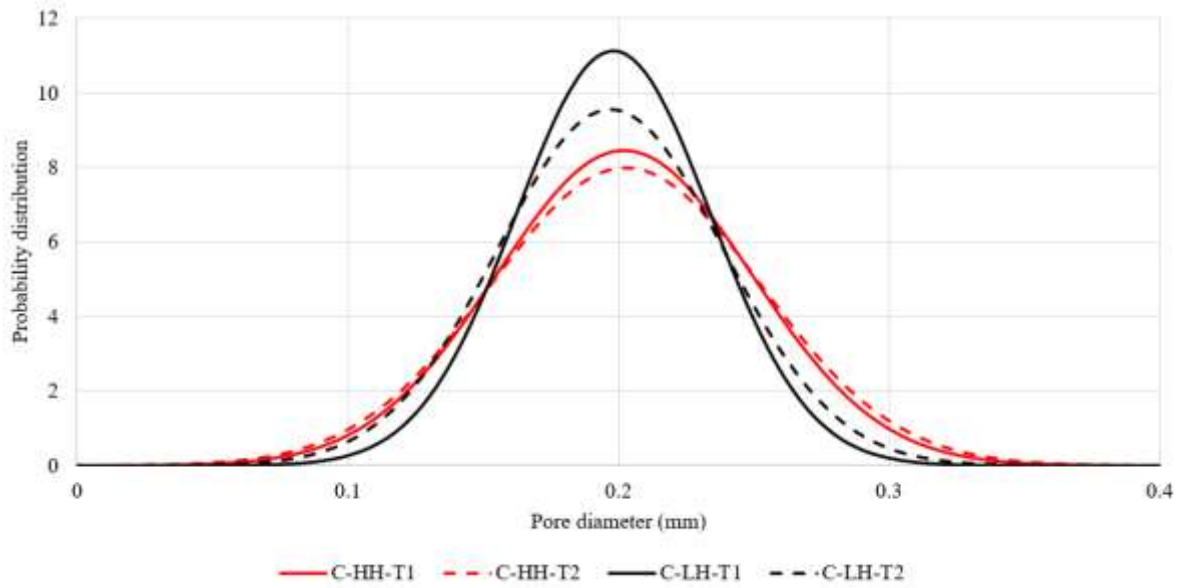
Fig 4 X-ray computed tomography of Samples (a) C-HH-T2 and (b) P-HH-T2.
Micrographs showing porosity morphology in respective samples (c) C-HH-T2 and
(d) P-HH-T2

1

2   **Fig 5 Count of different porosity size ranges in the samples manufactured with (a)**
3   **interlayer temperature control and (b) interlayer dwell time control**
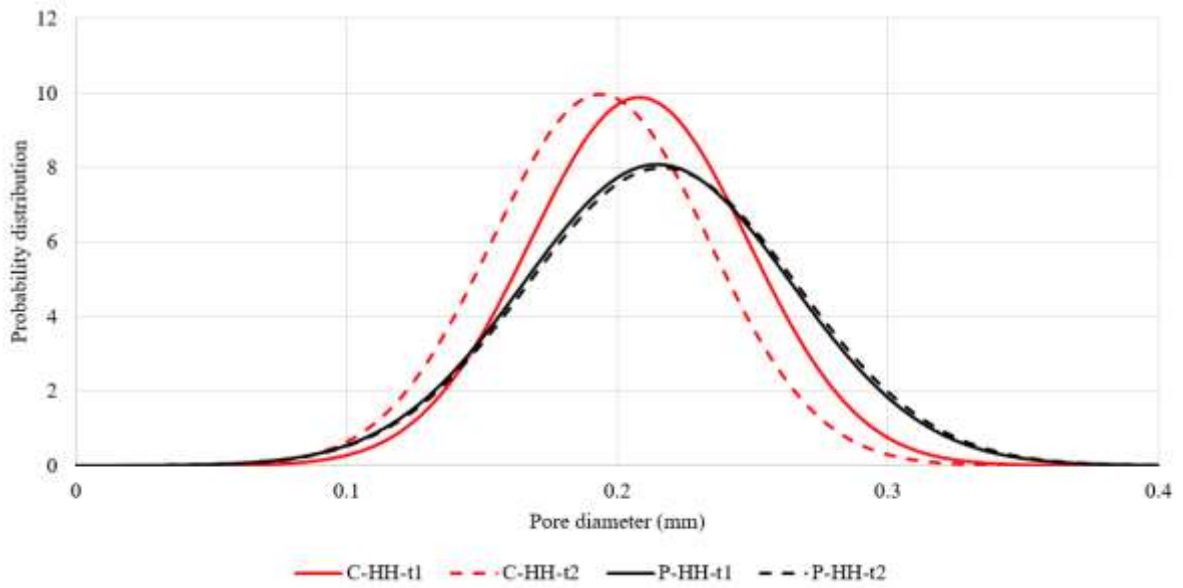
4

5

6

7

1

Fig 6 Effect of heat input and interlayer temperature on normal distribution of pore size in CMT samples (Set 2)
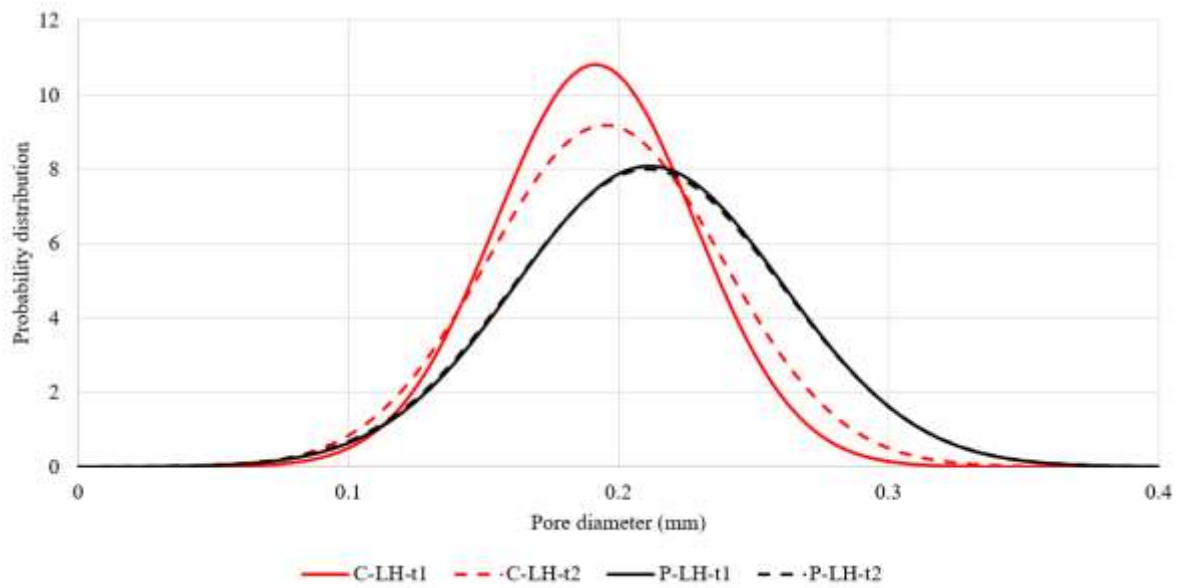

6

Fig 7 Effect of heat input and interlayer temperature on normal distribution of pore sizes in pulsed MIG samples (Set 1)
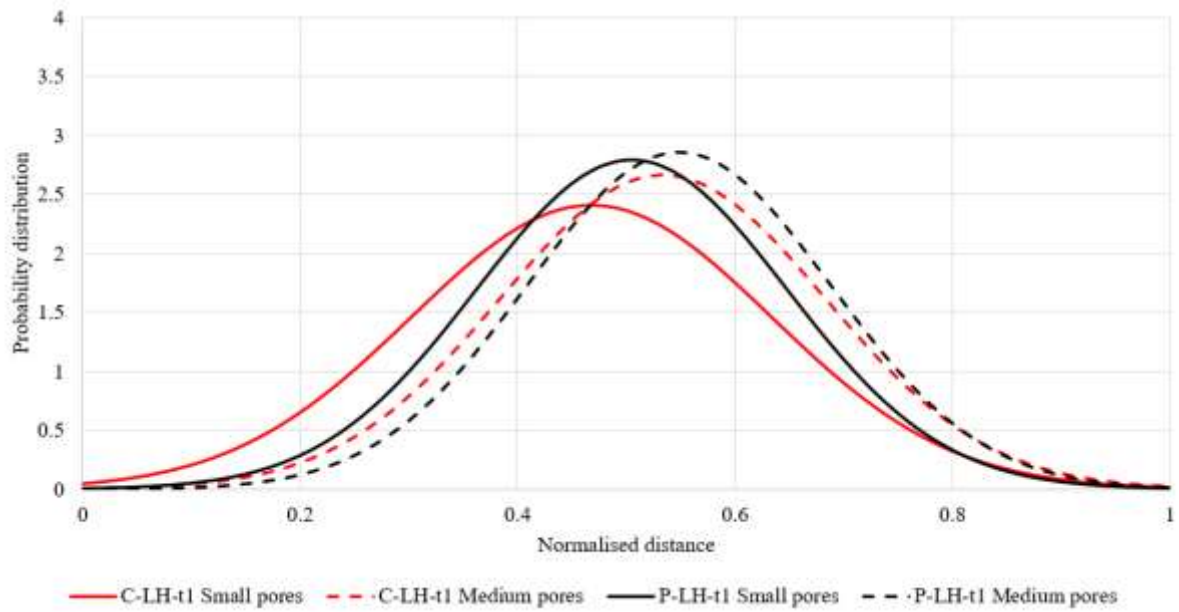
Fig 8 Effect metal deposition technique on normal distribution of pore size in samples manufactured with high heat input and different interlayer dwell time
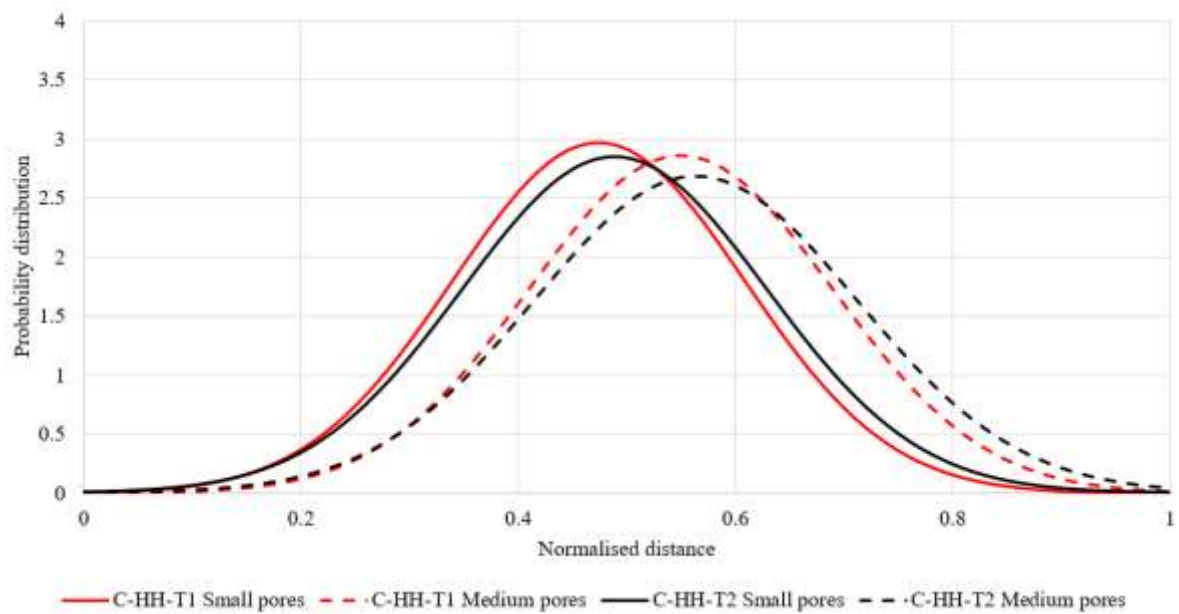

Fig 9 Effect metal deposition techniques on normal distribution of pore size in samples manufactured with low heat input and different interlayer dwell time
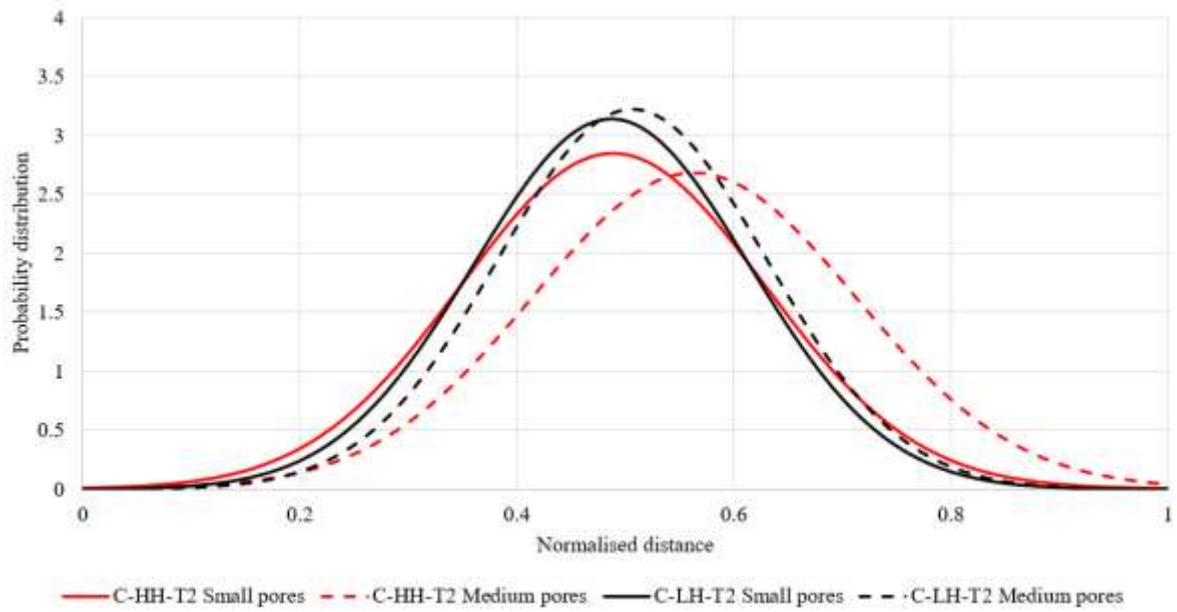
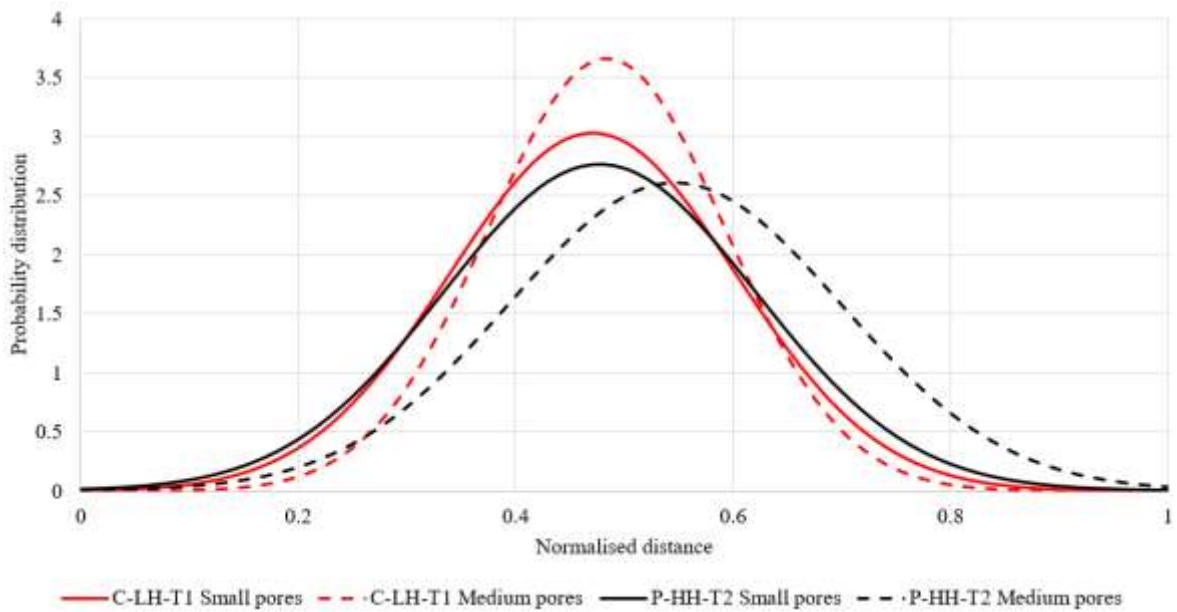**Fig 10 Effect of metal deposition technique on normal distribution of pore normalised distance between centroids**

Fig 11 Effect of interlayer temperature on normal distribution of pore normalised distances from centroid of all pores

Fig 12 Effect of heat input on normal distribution of pore normalised distances from centroid of all pores

Fig 13 Normal distribution of pore normalised distances from centroid of all pores for two difference metal deposition conditions

Fig 14 Volume fraction of different porosity size ranges in samples manufactured with (a) interlayer temperature control and (b) interlayer dwell time control

(a) (b) (c) (d)

Fig 15 Effect of metal deposition technique on penetration in schematic and macro form (a) and (c) showing pulsed MIG and (b) and (d) represented CMT

Pores formed at upper portion of layer

Pores trapped at interlayer regions

(a) (b)

Fig 16 XCT image of porosity distribution shown in the longitudinal direction of samples prepared using (a) CMT technique and (b) pulsed MIG process

Fig 17 Effect of pulsed MIG and CMT metal deposition techniques on hydrogen absorption

Table 1 Nominal chemical composition of depositing wire and substrate (in weight percentage)

Elements	Si	Mn	Cr	Cu	Ti	Fe	Zn	Mg	Al
Filler wire	0.06	0.65	0.07	0.01	0.07	0.14	<0.01	4.91	Balance
Substrate	0.11	0.66	0.06	0.05	0.05	0.25	0.05	4.74	Balance

Table 2 Parameters employed for manufacturing of test samples

Parameter	Pulsed metal inert gas (MIG)		Cold metal transfer (CMT)	
	Low heat input	High heat input	Low heat input	High heat input
Average Current (A)	73	152	73	152
Average Voltage (V)	18.3	18.7	18.2	19.2
Torch travel speed (m/min)	0.6		0.6	
Heat input (J/mm)	158	351	140	345
Wire feed speed (m/min)	4.85	8.65	4.9	8.6
Wire feed speed / travel speed	8.1	14.4	8.1	14.3

Table 3 Sample identification and set groups

Set no.	Metal deposition technique	Heat input	Interlayer temperature (T) / Interlayer dwell time (t)	Samples
1	Pulsed MIG (P)	High (HH) Low (LH)	50°C (T1) 100°C (T2)	P-HH-T1, P-HH-T2, P-LH-T1, P-LH-T2
2	CMT (C)	High (HH) Low (LH)	50°C (T1) 100°C (T2)	C-HH-T1, C-HH-T2, C-LH-T1, C-LH-T2
3	Pulsed MIG (P)	High (HH) Low (LH)	30 secs (t1) 120 secs (t2)	P-HH-t1, P-HH-t2, P-LH-t1, P-LH-t2
4	CMT (C)	High (HH) Low (LH)	30 secs (t1) 120 secs (t2)	C-HH-t1, C-HH-t2, C-LH-t1, C-LH-t2

Table 4 Pore volume fraction for samples manufactured with different interlayer temperatures (sets 1 and 2) or with different interlayer dwell time

Process	Heat input	Sample ID	Pore volume fraction % with respect to sample volume
Pulsed MIG (Set 1)	High	P-HH-T1	0.106
		P-HH-T2	0.063
	Low	P-LH-T1	0.152
		P-LH-T2	0.122
CMT (Set 2)	High	C-HH-T1	0.05
		C-HH-T2	0.057
	Low	C-LH-T1	0.031
		C-LH-T2	0.041
Pulsed MIG (Set 3)	High	P-HH-t1	0.066
		P-HH-t2	0.127
	Low	P-LH-t1	0.077
		P-LH-t2	0.175
CMT (Set 4)	High	C-HH-t1	0.07
		C-HH-t2	0.061
	Low	C-LH-t1	0.049
		C-LH-t2	0.038

Table 5 Comparison of pore size range and distribution for pulsed MIG and CMT aluminium samples

Pore diameter range (mm)	Pore count fraction (%)	
	Pulsed MIG	CMT
Small (0.11 – 0.20)	52.79 – 62.9	60.69 – 77.47
Medium (0.21 – 0.30)	32.34 – 42.36	20.0 – 35.59
Large (≥ 0.31)	3.3 – 5.78	1.15 – 4.63

Table 6 Comparison of hydrogen content obtained from dissolved hydrogen test in CMT and pulsed MIG samples

Set ID.	Process / technique	Sample ID	Pore volume fraction (%)	Detected hydrogen content (ppm)	Hydrogen content (ppm) / pore volume fraction (%) (ppm/volume %)
DH1	CMT	C-LH-T1	0.031	0.834	26.900
	Pulsed MIG	P-LH-T1	0.152	0.993	6.530
DH2	CMT	C-LH-t2	0.038	1.020	26.840
	Pulsed MIG	P-LH-t2	0.175	1.250	7.140

Table 11 Comparison of total hydrogen content, hydrogen in pores and dissolved hydrogen obtained from dissolved hydrogen test in samples prepared using CMT and pulsed MIG (refer Annexure)

Set ID	Samples ID	Total hydrogen in samples of 100 g (ml)	Percentage of hydrogen forming pores	Percentage of hydrogen in solid solution
DH1	C-LH-T1	0.934	1.220	98.780
	P-LH-T1	1.112	5.060	94.940
DH2	C-LH-t2	1.142	1.250	98.750
	P-LH-t2	1.400	4.480	95.520

Table A Details of dissolved hydrogen values samples wise

Samples ID	Weight of samples consumed in dissolved hydrogen test (g)	Total detected hydrogen in sample (ml)	Expected total hydrogen in samples of 100 g (ml)	Volume of hydrogen at pores (%)	Dissolved hydrogen volume in solid sample (%)
CBJ	0.402	0.003755	0.934	1.22	98.78
PBJ	0.5659	0.006293	1.112	5.06	94.94
CBZ	0.2899	0.003311	1.142	1.25	98.75
PBZ	0.5015	0.007021	1.4	4.48	95.52